Quantum phase transitions in a charge-coupled Bose-Fermi Anderson model

Mengxing Cheng,[1,*] Matthew T. Glossop,[2] and Kevin Ingersent[1]
[1]*Department of Physics, University of Florida, Gainesville, Florida 32611-8440, USA*
[2]*Physics and Astronomy Department, Rice University, 6100 Main Street, Houston, Texas 77005, USA*
(Received 30 July 2009; published 9 October 2009)

We study the competition between Kondo physics and dissipation within an Anderson model of a magnetic impurity level that hybridizes with a metallic host and is also coupled, via the impurity charge, to the displacement of a bosonic bath having a spectral density proportional to ω^s. As the impurity-bath coupling increases from zero, the effective Coulomb interaction between two electrons in the impurity level is progressively renormalized from its repulsive bare value until it eventually becomes attractive. For weak hybridization, this renormalization in turn produces a crossover from a conventional spin-sector Kondo effect to a charge Kondo effect. At particle-hole symmetry, and for sub-Ohmic bath exponents $0<s<1$, further increase in the impurity-bath coupling results in a continuous zero-temperature transition to a broken-symmetry phase in which the ground-state impurity occupancy $\hat{n}_d$ acquires an expectation value $\langle \hat{n}_d \rangle_0 \neq 1$. The response of the impurity occupancy to a locally applied electric potential features the hyperscaling of critical exponents and ω/T scaling that are expected at an interacting critical point. The numerical values of the critical exponents suggest that the transition lies in the same universality class as that of the sub-Ohmic spin-boson model. For the Ohmic case $s=1$, the transition is instead of Kosterlitz-Thouless type. Away from particle-hole symmetry, the quantum phase transition is replaced by a smooth crossover but signatures of the symmetric quantum critical point remain in the physical properties at elevated temperatures and/or frequencies.

DOI: 10.1103/PhysRevB.80.165113 PACS number(s): 71.10.Hf, 75.20.Hr, 73.43.Nq, 05.10.Cc

I. INTRODUCTION

Quantum impurity models have intrigued physicists for more than half a century.[1] In recent years, the focus has largely been on models that exhibit quantum phase transitions (QPTs). Strictly, these are *boundary* QPTs at which only a subset of system degrees of freedom becomes critical.[2] Boundary QPTs not only serve as prototypes for the bulk QPTs encountered (or postulated to exist) in many strongly correlated systems,[3,4] but in certain cases they are amenable to controlled realization in quantum-dot setups.[5]

Of great current interest are dissipative quantum impurity models that describe a dynamical local degree of freedom coupled to one or more bosonic modes representing a frictional environment. Experiments on single-molecule transistors[6] have drawn attention to transport through nanodevices featuring electron-phonon interactions as well as local electron-electron interactions. The essential physics of these experiments seems to be captured in variants[7–12] of the Anderson-Holstein model, which augments the Anderson impurity model[13] with a Holstein coupling of the impurity occupancy to a local (nondispersive) phonon mode. The Anderson-Holstein model has been studied since the 1970s in connection with the phenomenon of mixed valence[14–16] and has also been adapted to treat the effect of negative-U tunneling centers on superconductivity.[17,18] The many theoretical approaches that have been applied to these models have yielded general agreement that phonons serve to reduce the effective Coulomb repulsion between electrons in the impurity level, or even to produce an attractive net electron-electron interaction. Most challenging has been the study of simultaneous strong Coulomb repulsion and strong electron-phonon coupling. Here, the most robust solutions have been provided by an extension of the numerical renormalization-group (NRG) technique, long established as a reliable tool for tackling pure-fermionic quantum impurity problems.[19–21] NRG studies[8,10,15] have shown that in the one-channel Anderson-Holstein model, descriptive of a single molecule coupled symmetrically to source and drain leads, increasing the phonon coupling from zero results in a smooth crossover from a conventional Kondo effect, involving conduction-band screening of the impurity spin degree of freedom, to a predominantly charge Kondo effect in which it is the impurity "isospin" or deviation from half-filling that is quenched by the conduction band. However, even for very strong electron-phonon couplings, the ground state remains a many-body Kondo singlet and there is no QPT. By contrast, a two-channel model describing a single-molecular transistor with a center-of-mass vibrational mode exhibits a line of QPTs manifesting the critical physics of the two-channel Kondo model.[12]

An even greater theoretical challenge is posed by quantum impurities coupled to dispersive bosons. A canonical example is the spin-boson model,[22] which describes tunneling within a two-state system coupled to a bosonic bath. The model has many proposed applications, including frictional effects on biological and chemical reaction rates,[23] cold atoms in a quasi-one-dimensional optical trap,[24] a quantum dot coupled to Luttinger-liquid leads,[25] and study of entanglement between a qubit and its environment.[26,27] In many cases, the dissipative bosonic bath can be described by a spectral density [formally defined in Eq. (8) below] that is proportional to ω^s at low frequencies ω. The spin-boson model with an Ohmic ($s=1$) bath has long been known[22] to exhibit a Kosterlitz-Thouless QPT between delocalized and localized phases. The existence of a QPT for sub-Ohmic ($0<s<1$) baths was for some years the subject of debate.[22,28] However, clear evidence for a continuous QPT has been provided by the NRG,[27,29,30] by perturbative expansion in $\epsilon=s$

about the delocalized fixed point,[31] and through exact-diagonalization calculations.[32]

Theoretical activity has also centered on the Bose-Fermi Kondo (BFK) model,[33] in which an impurity spin-$\frac{1}{2}$ degree of freedom is coupled both to a fermionic band of conduction electrons and to one or more bosonic baths. BFK models arise in the context of unconventional heavy-fermion quantum criticality treated within extended dynamical mean-field theory (extended DMFT) (Ref. 34) and have also been proposed to describe quantum dots coupled either to a noisy environment[35] or to ferromagnetic leads.[36] Studies of BFK models having different spin rotation symmetry—SU(2), *XY*, or Ising—employing either expansion[37] in $\epsilon=1-s$ or the NRG (Refs. 38 and 39) have found continuous QPTs between phases exhibiting the Kondo effect and localized phases in which impurity spin flips are suppressed by the coupling to the bosonic bath(s). For exponents $0<s<1$, most evidence suggests that the continuous QPTs of the spin-boson and of Ising-anisotropic BFK models are equivalent. QPTs outside the spin-boson universality class have been identified in dissipative models featuring a pseudogap in the electronic density of states.[40]

In this paper, we combine the themes outlined in the preceding paragraphs by investigating a *charge-coupled Bose-Fermi Anderson (BFA) model* in which the impurity not only hybridizes with conduction-band electrons but also is coupled, via its electron occupancy, to a bath representing acoustic phonons or other bosonic degrees of freedom whose dispersion extends to zero energy. The model was introduced more than 30 years ago[41–43] in connection with the mixed-valence problem. A spinless version of the model was also discussed in the same context.[44] More recently, very similar models have been shown to arise as effective impurity problems in the extended DMFT for one- and two-band extended Hubbard models.[45,46] Hitherto, only limited progress has been made toward understanding the physics of such models, and we are aware of no study of their possible QPTs.

Our NRG study of the charge-coupled BFA model with bosonic baths characterized by exponents $0<s\leqslant 1$ reveals a crossover with increasing electron-boson (*e-b*) coupling from a spin Kondo effect to a charge Kondo effect, very similar to that noted previously in the Anderson-Holstein model.[8,10,15] However, under conditions of strict particle-hole symmetry, further increase in the *e-b* coupling leads to complete suppression of Kondo physics at a quantum critical point. Beyond the critical *e-b* coupling lies a localized phase in which charge fluctuations on the impurity site are frozen. For sub-Ohmic baths ($0<s<1$), the QPT is continuous and the numerical values of the critical exponents describing the response of the impurity charge to a locally applied electric potential demonstrate that the transition belongs to the same universality class as that of the spin-boson and Ising BFK models. For Ohmic baths (corresponding to $s=1$), the QPT is found to be of Kosterlitz-Thouless type. Particle-hole asymmetry acts in a manner analogous to a magnetic field at a conventional ferromagnetic ordering transition, smearing the discontinuous change in the ground state as a function of *e-b* coupling into a smooth crossover. Signatures of the symmetric quantum critical point remain in the physical properties at elevated temperatures and/or frequencies.

It is important to note that questions have been raised as to whether or not the NRG method reliably captures the quantum critical behavior of the spin-boson and Ising BFK models for bath exponents $0<s<\frac{1}{2}$. It is a standard belief[3,4] that the low-energy behavior near a quantum phase transition in d spatial dimensions is equivalent to that of a classical transition in $d+z$ dimensions, where z is the dynamical exponent. In the case of the spin-boson and Ising BFK models, for which $d=0$ and $z=1$, the corresponding classical system is a one-dimensional Ising chain with long-ranged interactions that decay for large separations r like $r^{-(1+s)}$. The Ising chain is known to possess an interacting critical point for $\frac{1}{2}<s<1$ but to exhibit a mean-field transition[49] for $0<s<\frac{1}{2}$. By contrast, NRG studies of the spin-boson[31] and Ising BFK (Refs. 38 and 39) models have found non-mean-field behavior extending over the entire range $0<s<1$, leading to a claim of breakdown of the quantum-to-classical mapping.[31] This claim has recently been contradicted by continuous-time Monte Carlo[50] and exact diagonalization[32] studies. Debate is ongoing concerning the interpretation of these various results.[50,51] The eventual resolution of this debate may determine the validity of the small subset of our NRG results that concerns the critical exponents of the charge-coupled BFA model with bath exponents $0<s<\frac{1}{2}$. There is every reason to believe that the remaining results are physically sound.

The rest of this paper is organized as follows. Section II introduces the charge-coupled BFA Hamiltonian and summarizes the NRG method used to solve the model. Section III contains a preliminary analysis of the model, focusing on the bosonic renormalization of the effective electron-electron interaction within the impurity level. Numerical results for the symmetric model with sub-Ohmic ($0<s<1$) dissipation are presented and interpreted in Sec. IV. Section V treats the symmetric model with Ohmic ($s=1$) dissipation. Section VI discusses the effects of particle-hole asymmetry. The paper's conclusions are presented in Sec. VII.

II. MODEL AND SOLUTION METHOD

A. Charge-coupled Bose-Fermi Anderson Hamiltonian and related models

In this work, we investigate the charge-coupled Bose-Fermi Anderson model described by the Hamiltonian

$$\hat{H}_{\mathrm{CCBFA}}=\hat{H}_{\mathrm{imp}}+\hat{H}_{\mathrm{band}}+\hat{H}_{\mathrm{bath}}+\hat{H}_{\mathrm{imp\text{-}band}}+\hat{H}_{\mathrm{imp\text{-}bath}}, \quad (1)$$

where

$$\hat{H}_{\mathrm{imp}}=\epsilon_d\hat{n}_d+U\hat{n}_{d\uparrow}\hat{n}_{d\downarrow}, \quad (2)$$

$$\hat{H}_{\mathrm{band}}=\sum_{\mathbf{k},\sigma}\epsilon_{\mathbf{k}}c^{\dagger}_{\mathbf{k}\sigma}c_{\mathbf{k}\sigma}, \quad (3)$$

$$\hat{H}_{\mathrm{bath}}=\sum_{\mathbf{q}}\omega_{\mathbf{q}}a^{\dagger}_{\mathbf{q}}a_{\mathbf{q}}, \quad (4)$$

$$\hat{H}_{\mathrm{imp\text{-}band}}=\frac{1}{\sqrt{N_k}}\sum_{\mathbf{k},\sigma}\left(V_{\mathbf{k}}c^{\dagger}_{\mathbf{k}\sigma}d_{\sigma}+V^{*}_{\mathbf{k}}d^{\dagger}_{\sigma}c_{\mathbf{k}\sigma}\right), \quad (5)$$

$$\hat{H}_{\text{imp-bath}} = \frac{1}{\sqrt{N_q}}(\hat{n}_d - 1)\sum_{\mathbf{q}} \lambda_{\mathbf{q}}(a_{\mathbf{q}} + a^{\dagger}_{-\mathbf{q}}). \tag{6}$$

Here, d_σ annihilates an electron of spin z component $\sigma = \pm\frac{1}{2}$ (or $\sigma = \uparrow, \downarrow$) and energy $\epsilon_d < 0$ in the impurity level, $\hat{n}_{d\sigma} = d^{\dagger}_{\sigma} d^{\dagger}_{\sigma}$, $\hat{n}_d = \hat{n}_{d\uparrow} + \hat{n}_{d\downarrow}$, and $U > 0$ is the Coulomb repulsion between two electrons in the impurity level. $V_{\mathbf{k}}$ is the hybridization between the impurity and a conduction-band state of energy $\epsilon_{\mathbf{k}}$ annihilated by fermionic operator $c_{\mathbf{k}\sigma}$, and $\lambda_{\mathbf{q}}$ characterizes the coupling of the impurity occupancy to bosons in an oscillator state of energy $\omega_{\mathbf{q}}$ annihilated by operator $a_{\mathbf{q}}$. N_k is the number of unit cells in the host metal and, hence, the number of inequivalent $\mathbf{k}$ values. Correspondingly, N_q is the number of oscillators in the bath, and the number of distinct values of $\mathbf{q}$. Without loss of generality, we take $V_{\mathbf{k}}$ and $\lambda_{\mathbf{q}}$ to be real and non-negative. Throughout the paper, we drop all factors of the reduced Planck constant $\hbar$, Boltzmann's constant k_B, the impurity magnetic moment $g\mu_B$, and the electronic charge e.

To focus on the most interesting physics of the model, we assume a constant hybridization $V_{\mathbf{k}} = V$ and a flat conduction-band density of states (per unit cell, per spin-z orientation)

$$\rho(\epsilon) \equiv \frac{1}{N_k}\sum_{\mathbf{k}} \delta(\epsilon - \epsilon_{\mathbf{k}}) = \begin{cases} \rho_0 = (2D)^{-1} & \text{for } |\epsilon| < D \\ 0 & \text{otherwise,} \end{cases} \tag{7}$$

defining the hybridization width $\Gamma = \pi\rho_0 V^2$. The bosonic bath is completely specified by its spectral density, which we take to have the pure power-law form

$$B(\omega) \equiv \frac{\pi}{N_q}\sum_{\mathbf{q}} \lambda^2_{\mathbf{q}}\delta(\omega - \omega_{\mathbf{q}}) = \begin{cases} (K_0\lambda)^2\Omega^{1-s}\omega^s & \text{for } 0 < \omega < \Omega \\ 0 & \text{otherwise,} \end{cases} \tag{8}$$

characterized by an upper cutoff Ω, an exponent s that must satisfy $s > -1$ to ensure normalizability, and a dimensionless prefactor $K_0\lambda$. In this paper, we present results only for the case $\Omega = D$ in which the bath and band share a common cutoff. We also adopt the convention that K_0 is held constant while one varies λ, which we term the electron-boson (e-b) coupling. It should be emphasized, though, that the key features of the model are a nonvanishing Fermi-level density of states $\rho(0) > 0$ and the asymptotic behavior $B(\omega) \propto \omega^s$ for $\omega \to 0$. Relaxing any or all of the remaining assumptions laid out in this paragraph will not alter the essential physics of the model, although it may affect nonuniversal properties, such as the locations of phase boundaries.

For many purposes, it is convenient to rewrite[20] the impurity part of the Hamiltonian (dropping a constant term ϵ_d)

$$\hat{H}_{\text{imp}} = \delta_d(\hat{n}_d - 1) + \frac{U}{2}(\hat{n}_d - 1)^2, \tag{9}$$

where $\delta_d = \epsilon_d + U/2$. Most of the results presented below were obtained for the symmetric model characterized by $\epsilon_d = -U/2$ or $\delta_d = 0$, for which the impurity states $n_d = 0$ and $n_d = 2$ are degenerate in energy. Section VI addresses the behavior of the asymmetric model.

In any realization of $\hat{H}_{\text{CCBFA}}$ involving coupling of acoustic phonons to a magnetic impurity or a quantum dot, the value of the bath exponent s will depend on the precise interaction mechanism. However, phase space considerations suggest that any such system will lie in the super-Ohmic regime $s > 1$. Models closely related to $\hat{H}_{\text{CCBFA}}$ have also been considered in the context of extended DMFT,[46,47] a technique for systematically incorporating some of the spatial correlations that are omitted from the conventional DMFT of lattice fermions.[48] Extended DMFT maps the lattice problem onto a quantum impurity problem in which a central site interacts with both a fermionic band and one or more bosonic baths, the latter representing fluctuating effective fields due to interactions between different lattice sites. The charge-coupled BFA model serves as the mapped impurity problem for various extended Hubbard models with nonlocal density-density interactions.[45,46] In these settings, the effective bath exponent s is not known *a priori* but is determined through self-consistency conditions that ensure that the central site is representative of the lattice as a whole. The extended DMFT treatment of other lattice models[34] gives rise to exponents $0 < s < 1$, and we expect this also to be the case for the extended Hubbard models.

At the Hartree-Fock level,[42] the impurity properties of Hamiltonian (1) are identical to those of the Anderson-Holstein Hamiltonian,

$$\hat{H}_{\text{AH}} = \hat{H}_{\text{A}} + \omega_0 a^{\dagger}a + \lambda_0(\hat{n}_d - 1)(a + a^{\dagger}), \tag{10}$$

which augments the well-studied Anderson impurity model,[13]

$$\hat{H}_{\text{A}} = \hat{H}_{\text{imp}} + \hat{H}_{\text{band}} + \hat{H}_{\text{imp-band}}, \tag{11}$$

with a Holstein coupling of the impurity charge to a single phonon mode of energy ω_0. At several points in the sections that follow, we compare and contrast our results for $\hat{H}_{\text{CCBFA}}$ with those obtained previously for $\hat{H}_{\text{AH}}$.

B. Numerical renormalization-group method

We solve the charge-coupled BFA model using the NRG method,[19–21] as recently extended to treat models involving both dispersive bosons and dispersive fermions.[38,39] The full range of conduction-band energies $-D < \epsilon < D$ (bosonic-bath energies $0 < \omega < \Omega$) is divided into a set of logarithmic intervals bounded by $\epsilon = \pm D\Lambda^{-k}$ ($\omega = \Omega\Lambda^{-k}$) for $k = 0, 1, 2, \ldots$, where $\Lambda > 1$ is the Wilson discretization parameter. The continuum of states within each interval is replaced by a single state, namely, the particular linear combination of band (bath) states within the interval that enters $\hat{H}_{\text{imp-band}}$ ($\hat{H}_{\text{imp-bath}}$). The discretized model is then transformed into a tight-binding form involving two sets or orthonormalized operators: (i) $f_{n\sigma}$ ($n = 0, 1, 2, \ldots$) constructed as linear combinations of all $c_{\mathbf{k}\sigma}$ having $|\epsilon_{\mathbf{k}}| < D\Lambda^{-n}$ and (ii) b_m ($m = 0, 1, 2, \ldots$) mixing all $a_{\mathbf{q}}$ such that $0 < \omega_{\mathbf{q}} < \Omega\Lambda^{-m}$. This procedure maps the last four parts of Hamiltonian (1) to

$$\hat{H}_{\text{band}}^{\text{NRG}} = D\sum_{n=0}^{\infty}\sum_{\sigma}[\epsilon_n f_{n\sigma}^{\dagger} f_{n\sigma} + \tau_n(f_{n\sigma}^{\dagger} f_{n-1,\sigma} + f_{n-1,\sigma}^{\dagger} f_{n\sigma})], \tag{12}$$

$$\hat{H}_{\text{bath}}^{\text{NRG}} = \Omega\sum_{m=0}^{\infty}[e_m b_m^{\dagger} b_m + t_m(b_m^{\dagger} b_{m-1} + b_{m-1}^{\dagger} b_m)], \tag{13}$$

$$\hat{H}_{\text{imp-band}}^{\text{NRG}} = \sqrt{\frac{2\Gamma D}{\pi}}(f_{0\sigma}^{\dagger} d_{\sigma} + d_{\sigma}^{\dagger} f_{0\sigma}), \tag{14}$$

$$\hat{H}_{\text{imp-bath}}^{\text{NRG}} = \frac{\Omega K_0 \lambda}{\sqrt{\pi(s+1)}}(\hat{n}_d - 1)(b_0 + b_0^{\dagger}). \tag{15}$$

Here, $\tau_0 = t_0 = 0$, while the remaining coefficients ϵ_n, τ_n, e_m, and t_m, which include all information about the conduction-band density of states $\rho(\epsilon)$ and the bosonic spectral density $B(\omega)$, are calculated via Lanczos recursion relations.[39] For a particle-hole-symmetric density of states such as that in Eq. (7), $\epsilon_n = 0$ for all n.

The coefficients τ_n in Eq. (12) vary for large n as $D\Lambda^{-n/2}$, while e_m and t_m entering Eq. (13) vary for large m as $\Omega\Lambda^{-m}$. Therefore, the problem can be solved iteratively by diagonalization of a sequence of Hamiltonians $\hat{H}_N$ $(N = 0, 1, 2, \ldots)$ describing tight-binding chains of increasing length. At iteration $N \geqslant 0$, Eq. (12) is restricted to $0 \leqslant n \leqslant N$, while Eq. (13) is limited to $0 \leqslant m \leqslant M(N)$. The spirit of the NRG is to treat fermions and bosons of the same energy scale at the same iteration. Since the bosonic coefficients decay with site index twice as fast as the fermionic coefficients, after a few iterations the iterative procedure requires extension of the bosonic chain only for every second site added to the fermionic chain. In this work, we have chosen for simplicity to work with a single high-energy cutoff scale $D \equiv \Omega$. It is then convenient to add to the bosonic chain at every even-numbered iteration so that the highest-numbered bosonic site is $M(N) = \lfloor N/2 \rfloor$, where $\lfloor x \rfloor$ is the greatest integer less than or equal to x.

The NRG method relies on two additional approximations. Even for pure-fermionic problems, it is not feasible to keep track of all the eigenstates because the dimension of the Fock space increases rapidly as we add sites to the chains. Therefore, only the lowest lying N_s many-particle states can be retained after each iteration. The presence of bosons adds the further complication that the Fock space is infinite-dimensional even for a single-site chain, making it necessary to restrict the maximum number of bosons per chain site to a finite number N_b. Provided that N_s and N_b are chosen to be sufficiently large (as discussed in Sec. IV A), the NRG solution at iteration N provides a good account of the impurity contribution to physical properties at temperatures T and frequencies ω of order $D\Lambda^{-N/2}$.

Hamiltonian (1) commutes with the total spin-z operator

$$\hat{S}_z = \frac{1}{2}(\hat{n}_{d\uparrow} - \hat{n}_{d\downarrow}) + \frac{1}{2}\sum_n (f_{n\uparrow}^{\dagger} f_{n\uparrow} - f_{n\downarrow}^{\dagger} f_{n\downarrow}), \tag{16}$$

the total spin-raising operator

$$\hat{S}_+ = d_{\uparrow}^{\dagger} d_{\downarrow} + \sum_n f_{n\uparrow}^{\dagger} f_{n\downarrow} \equiv (\hat{S}_-)^{\dagger}, \tag{17}$$

and the total "charge" operator

$$\hat{Q} = \hat{n}_d - 1 + \sum_n (f_{n\uparrow}^{\dagger} f_{n\uparrow} + f_{n\downarrow}^{\dagger} f_{n\downarrow} - 1), \tag{18}$$

which measures the deviation from half-filling of the total electron number. One can interpret

$$\hat{I}_z = \frac{1}{2}\hat{Q}, \quad \hat{I}_+ = -d_{\uparrow}^{\dagger} d_{\downarrow}^{\dagger} + \sum_n (-1)^n f_{n\uparrow}^{\dagger} f_{n\downarrow}^{\dagger} \equiv (\hat{I}_-)^{\dagger} \tag{19}$$

as the generators of an SU(2) isospin symmetry (originally dubbed "axial charge" in Ref. 53). Since $[\hat{H}_{\text{imp-bath}}, \hat{I}_{\pm}] \neq 0$, the charge-coupled BFA model does not exhibit full isospin symmetry. However, this symmetry turns out to be recovered in the asymptotic low-energy behavior at certain renormalization-group fixed points.

As described in Ref. 20, the computational effort required for the NRG solution of a problem can be greatly reduced by taking advantage of these conserved quantum numbers. In particular, it is possible to obtain all physical quantities of interest while working with a reduced basis of simultaneous eigenstates of $\hat{S}^2$, $\hat{S}_z$, and $\hat{Q}$ with eigenvalues satisfying $S_z = S$. With one exception noted in Sec. IV G, any N_s value specified below represents the number of retained (S, Q) multiplets, corresponding to a considerably larger number of (S, S_z, Q) states.

Even when advantage is taken of all conserved quantum numbers, NRG treatment of the charge-coupled BFA model remains much more demanding than that of the Anderson model [Eq. (11)] or the Anderson-Holstein model [Eq. (10)]. Being nondispersive, the bosons in the last model enter only the atomic-limit Hamiltonian $\hat{H}_0$, allowing solution via the standard NRG iteration procedure. For Bose-Fermi models such as $\hat{H}_{\text{CCBFA}}$, the need to extend a bosonic chain as well as a fermionic one at every even-numbered iteration $N > 0$ expands the basis of $\hat{H}_N$ from $4N_s$ states to $4(N_b+1)N_s$ states and multiplies the CPU time by a factor $\sim(N_b+1)^3$. Since we typically use $N_b = 8$ or 12 in our calculations, the increase in computational effort is considerable.

The choice of value for the NRG discretization parameter Λ involves trade-offs between discretization error (minimized by taking Λ to be not much greater than 1) and truncation error (reduced by working with $\Lambda \gg 1$). Experience from other problems[38,39,52] indicates that critical exponents can be determined very accurately using quite a large Λ. Most of the results presented in the remaining sections of the paper were obtained for $\Lambda = 9$, with $\Lambda = 3$ being employed in the calculation of the impurity spectral function. For convenience in displaying these results, we set $\Omega = D = 1$ and omit all factors of ρ_0 and K_0.

III. PRELIMINARY ANALYSIS

We begin by examining the special cases in which the impurity level is decoupled either from the conduction band

or from the bosonic bath. Understanding these cases allows us to establish some expectations for the behavior of the full model described by Eq. (1).

A. Zero hybridization

If one sets $\Gamma=0$ in Eq. (1), then the conduction band completely decouples from the remaining degrees of freedom and can be dropped from the model, leaving the zero-hybridization model

$$\hat{H}_{\mathrm{ZH}} = \delta_d(\hat{n}_d - 1) + \frac{U}{2}(\hat{n}_d - 1)^2 + \sum_{\mathbf{q}} \omega_{\mathbf{q}} a_{\mathbf{q}}^{\dagger} a_{\mathbf{q}} + \frac{1}{\sqrt{N_q}}(\hat{n}_d - 1)\sum_{\mathbf{q}} \lambda_{\mathbf{q}}(a_{\mathbf{q}} + a_{-\mathbf{q}}^{\dagger}). \tag{20}$$

The Fock space separates into sectors of fixed impurity occupancy ($n_d=0$, 1, or 2), within each of which the Hamiltonian can be recast, using displaced-oscillator operators

$$\bar{a}_{n_d,\mathbf{q}} = a_{\mathbf{q}} + \frac{\lambda_{\mathbf{q}}}{\sqrt{N_q}\omega_{\mathbf{q}}}(n_d - 1), \tag{21}$$

in the trivially solvable form

$$\hat{H}_{\mathrm{ZH}}(n_d) = \hat{H}'_{\mathrm{imp}} + \sum_{\mathbf{q}} \omega_{\mathbf{q}} \bar{a}^{\dagger}_{n_d,\mathbf{q}} \bar{a}_{n_d,\mathbf{q}}, \tag{22}$$

where

$$\hat{H}'_{\mathrm{imp}} = \delta_d(\hat{n}_d - 1) + \frac{U_{\mathrm{eff}}}{2}(\hat{n}_d - 1)^2. \tag{23}$$

The bosons act on the impurity to reduce the Coulomb interaction from its bare value U to an effective value

$$U_{\mathrm{eff}} = U - \frac{2}{N_q}\sum_{\mathbf{q}} \frac{\lambda_{\mathbf{q}}^2}{\omega_{\mathbf{q}}} = U - \frac{2}{\pi}\int_0^{\infty} \frac{B(\omega)}{\omega} d\omega. \tag{24}$$

For the bath spectral density in Eq. (8) with $-1 < s \leqslant 0$, one finds that for any nonzero e-b coupling λ, $U_{\mathrm{eff}}=-\infty$ and the singly occupied impurity states drop out of the problem. For the remainder of this section, however, we will instead focus on bath exponents $s>0$, for which Eqs. (8) and (24) give

$$U_{\mathrm{eff}} = U - \frac{2(K_0\lambda)^2}{\pi s}\Omega. \tag{25}$$

For weak e-b couplings, U_{eff} is positive and the ground state of $\hat{H}_{\mathrm{ZH}}$ lies in the sector $n_d=1$ where the impurity has a spin z component $\pm\frac{1}{2}$. However, U_{eff} is driven negative for sufficiently large λ, placing the ground state in the sector $n_d=0$ or $n_d=2$ where the impurity is spinless but has a charge (relative to half filling) of -1 or $+1$.

Figure 1 illustrates this renormalization of the Coulomb interaction for the symmetric model ($\delta_d=0$), in which the $n_d=0$ and $n_d=2$ states always have the same energy. In this case, all four impurity states become degenerate at a crossover e-b coupling

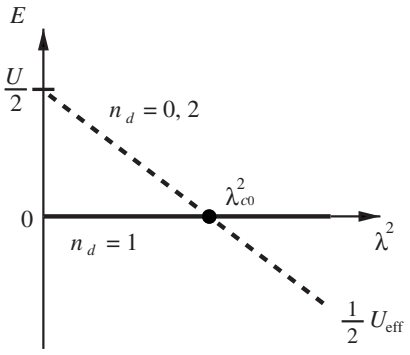

FIG. 1. Symmetric zero-hybridization model defined by $\hat{H}_{\mathrm{ZH}}$ in Eq. (20) with $\delta_d=0$: evolution with e-b coupling λ^2 of the lowest eigenenergy in the spin sector ($n_d=1$, solid line) and in the charge sector ($n_d=0,2$, dashed line). A level crossing occurs at $\lambda=\lambda_{c0}$ specified in Eq. (26).

$$K_0\lambda_{c0} = \sqrt{\pi s U/2\Omega}. \tag{26}$$

The impurity contributions to physical properties at this special point, which is characterized by effective parameters $\Gamma = U = \epsilon_d = 0$, are identical to those at the *free-orbital* fixed point[20] of the Anderson model.

For the general case of an asymmetric impurity, the sectors $n_d=0$ and 2 have a ground-state energy difference $E_0(n_d=2)-E_0(n_d=0)=2\delta_d$ for any value of λ. The overall ground state of Eq. (20) is a doublet ($n_d=1$, $S=\pm\frac{1}{2}$) for small e-b couplings, crossing over to a singlet ($n_d=0$ for $\delta_d>0$ or $n_d=2$ for $\delta_d<0$) for large λ. At $K_0\lambda_{c0} = \sqrt{\pi s(U/2-|\delta_d|)/\Omega}$, a point of threefold ground-state degeneracy, the impurity contributions to low-temperature ($T \ll |\delta_d|$) physical properties are identical to those at the *valence-fluctuation* fixed point[20] of the Anderson model.

Using the NRG with only a bosonic chain [Eq. (13)] coupled to the impurity site, we have confirmed the existence for $\delta_d=0$ of a simple level crossing from a spin-doublet ground state for $\lambda<\lambda_{c0}$ to a charge-doublet ground state for $\lambda>\lambda_{c0}$. In the former regime, the bosons couple only to the high-energy ($n_d=0,2$) impurity states, so the low-lying spectrum is that of free bosons obtained by diagonalizing $H_{\mathrm{bath}}^{\mathrm{NRG}}$ given in Eq. (13). Here, NRG truncation plays a negligible role provided that one works with $N_b \geqslant 8$ (say).

For $\lambda>\lambda_{c0}$, the low-lying bosonic excitations should, in principle, correspond to noninteracting displaced oscillators having precisely the same spectrum as the original bath. However, the occupation number $a_{\mathbf{q}}^{\dagger}a_{\mathbf{q}}$ in the ground state of Eq. (22) obeys a Poisson distribution with mean $\lambda_{\mathbf{q}}^2/(N_q\omega_{\mathbf{q}}^2)$. Thus, the total number of bosons corresponding to operators $a_{\mathbf{q}}$ satisfying $\Omega\Lambda^{-(k+1)} < \omega_{\mathbf{q}} < \Omega\Lambda^{-k}$ takes a mean value

$$\langle \hat{n}_k \rangle_0 = \int_{\Omega\Lambda^{-(k+1)}}^{\Omega\Lambda^{-k}} d\omega \frac{B(\omega)}{\pi\omega^2} = \begin{cases} \dfrac{(K_0\lambda)^2}{\pi}\ln\Lambda & \text{for } s=1 \\ \dfrac{(K_0\lambda)^2}{\pi}\dfrac{(\Lambda^{1-s}-1)}{(1-s)}\Lambda^{(1-s)k} & \text{otherwise.} \end{cases} \tag{27}$$

The bath states in the kth interval are represented by NRG chain states $0 \leqslant m \leqslant k$, with the greatest weight being borne by state $m=k$. Thus, a faithful representation of the displaced-oscillator spectrum requires inclusion of states having $b_m^\dagger b_m$ up to several times $\langle \hat{n}_m \rangle_0$; based on experience with the Anderson-Holstein model,[15] one expects $N_b \geqslant 4\langle \hat{n}_m \rangle_0$ to suffice. Given that $\langle \hat{n}_m \rangle_0 \propto \Lambda^{(1-s)m}$, it is feasible to meet this condition as $m \to \infty$ so long as the bath exponent satisfies $s \geqslant 1$. Indeed, for Ohmic and super-Ohmic bath exponents, the NRG spectrum for λ not too much greater than λ_{c0} is found to be numerically indistinguishable from that for $\lambda=0$. For $s<1$, by contrast, the restriction $b_m^\dagger b_m \leqslant N_b$ leads, for $\lambda > \lambda_{c0}$ and large iteration numbers, to an artificially truncated spectrum that cannot reliably access the low-energy physical properties. Nonetheless, observation of this "localized" bosonic spectrum serves as a useful indicator, both in the zero-hybridization limit and in the full charge-coupled BFA model, that the effective e-b coupling remains nonzero.

Another interpretation of Eq. (27) is that at the energy scale $E=\Omega\Lambda^{-k}$ characteristic of interval k, the e-b coupling takes an effective value $\tilde{\lambda}(E)$ governed by the renormalization-group equation

$$\frac{d\tilde{\lambda}}{d\ln(\Omega/E)} = \frac{1-s}{2}\tilde{\lambda}, \tag{28}$$

which implies that the e-b coupling is irrelevant for $s>1$, marginal for $s=1$, and relevant for $s<1$. While the NRG method is capable of faithfully reproducing the physics of $\hat{H}_{\mathrm{CCBFA}}$ for arbitrary renormalizations of ϵ_d, U, and Γ, its validity is restricted to the region

$$(K_0\tilde{\lambda})^2 \lesssim \frac{\pi N_B}{4}\frac{1-s}{\Lambda^{1-s}-1} \xrightarrow{\Lambda\to 1} \frac{\pi N_B}{4\ln\Lambda}. \tag{29}$$

For $\Lambda=9$ and $N_B=8$, as used in most of our calculations, the upper limit on the "safe" range of $K_0\tilde{\lambda}$ varies from 1.7 for $s=1$ to 0.9 for $s=0$.

We now focus on the value of the crossover e-b coupling λ_{c0} determined using the NRG approach. Figure 2 shows for five different bosonic bath exponents s that $K_0\lambda_{c0}$ has an almost linear dependence on the NRG discretization Λ in the range $1.6 \leqslant \Lambda \leqslant 4$. We believe that the rise in $K_0\lambda_{c0}$ with Λ reflects a reduction in the effective value of K_0 arising from the NRG discretization. It is known[20] that in NRG calculations for fermionic problems, the conduction-band density of states at the Fermi energy takes an effective value

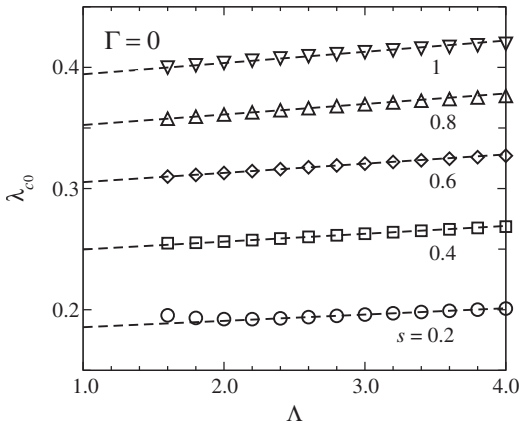

FIG. 2. Dependence of the level-crossing coupling λ_{c0} on the discretization Λ for the NRG solution of $\hat{H}_{\mathrm{ZH}}$ [Eq. (20)] with $U=0.1$, $\delta_d=0$, $N_s=200$, $N_b=16$, and five different values of the bath exponent s. Dashed lines show linear fits to the data.

$$\rho(0) = \bar{\rho}_0 = \rho_0/A_\Lambda, \tag{30}$$

where

$$A_\Lambda = \frac{\ln\Lambda}{2}\frac{1+\Lambda^{-1}}{1-\Lambda^{-1}}. \tag{31}$$

The general trend of the data in Fig. 2 is consistent with there being an analogous reduction in the bosonic bath spectral density that requires the replacement of K_0 by

$$\bar{K}_0 = K_0/A_{\Lambda,s} \tag{32}$$

when extrapolating NRG results to the continuum limit $\Lambda=1$. However, we have not obtained a closed-form expression for $A_{\Lambda,s}$.

Table I lists values $\lambda_{c0}(\Lambda\to 1)$ extrapolated from the data plotted in Fig. 2. For $s \geqslant 0.4$, these values are in good agreement with Eq. (26). For $s=0.2$, however, the extrapolated value of λ_{c0} lies significantly above the exact value, indicating that for given λ the NRG underestimates the bosonic renormalization of U. This is most likely another consequence of truncating the basis on each site of the bosonic tight-binding chain.

In analyzing our NRG results for the full charge-coupled BFA model, we attempt to compensate for the effects of discretization and truncation by replacing Eq. (25) by

TABLE I. Crossover coupling λ_{c0} for $\hat{H}_{\mathrm{ZH}}$ [Eq. (20)] with $U=0.1$, $\delta_d=0$, and five different values of the bath exponent s: comparison between λ_{c0}(exact) given by Eq. (26) and $\lambda_{c0}(\Lambda\to 1)$, the extrapolation to the continuum limit of numerical values obtained for $N_s=200$, $N_b=16$, and $1.6 \leqslant \Lambda \leqslant 4$. Parentheses surround the estimated nonsystematic error in the last digit.

s	0.2	0.4	0.6	0.8	1.0
λ_{c0}(exact)	0.177	0.251	0.307	0.355	0.396
$\lambda_{c0}(\Lambda\to 1)$	0.188(4)	0.250(2)	0.307(2)	0.355(2)	0.397(3)

$$U_{\rm eff}^{\rm NRG} = U[1 - (\lambda/\lambda_{c0})^2]. \tag{33}$$

Here, λ_{c0} is not the theoretical value predicted in Eq. (26) but rather is obtained from runs carried out for $\Gamma = 0$ but otherwise using the same model and NRG parameters as the data that are being interpreted.

B. Zero electron-boson coupling

For $\lambda = 0$, the bosonic bath decouples from the electronic degrees of freedom, which are then described by the pure Anderson model. In this section, we briefly review aspects of the Anderson model that will prove important in interpreting results for the charge-coupled BFA model. For further details concerning the Anderson model, see Refs. 1 and 20.

For any $\Gamma>0$, and for any U and $\delta_d \equiv \epsilon_d + U/2$ (whether positive, negative, or zero), the stable low-temperature regime of the Anderson model lies on a line of *strong-coupling* fixed points corresponding to $\Gamma=\infty$. At any of these fixed points, the system is locked into the ground state of the atomic Hamiltonian $\hat{H}_0$, and there are no residual degrees of freedom on the impurity site or on site $n=0$ of the fermionic chain; the NRG excitation spectrum is that of the Hamiltonian[20]

$$\hat{H}_{\rm SC}^{\rm NRG}(V_1) = D\sum_{n=1}^{\infty}\sum_{\sigma}\tau_n(f_{n\sigma}^{\dagger}f_{n-1,\sigma} + f_{n-1,\sigma}^{\dagger}f_{n\sigma}) + V_1\left(\sum_{\sigma} f_{1\sigma}^{\dagger}f_{1\sigma} - 1\right). \tag{34}$$

The coefficients τ_n are identical to those entering $\hat{H}_{\rm band}^{\rm NRG}$ [Eq. (12)], except that here $\tau_1=0$. Note that in Eq. (34), the sum over n begins at 1 rather than 0.

As shown in Ref. 20, the strong-coupling fixed points of the Anderson model are equivalent—apart from a shift of 1 in the ground-state charge Q defined in Eq. (18)—to the line of *frozen-impurity* fixed points corresponding to $\epsilon_d=\infty$, $\Gamma=U=0$, with NRG excitation spectra described by

$$\hat{H}_{\rm FI}^{\rm NRG}(V_0) = \hat{H}_{\rm band}^{\rm NRG} + V_0\left(\sum_{\sigma} f_{0\sigma}^{\dagger}f_{0\sigma} - 1\right). \tag{35}$$

The mapping between alternative specifications of the same fixed-point spectrum is[20]

$$\pi\bar{\rho}_0 V_0 = -(\pi\bar{\rho}_0 V_1)^{-1}, \tag{36}$$

where $\bar{\rho}_0$ [see Eq. (30)] is the effective conduction-band density of states.

The fixed-point potential scattering is related to the ground-state impurity charge via the Friedel sum rule,

$$\langle \hat{n}_d - 1\rangle_0 = \frac{2}{\pi}\,\mathrm{arccot}(\pi\bar{\rho}_0 V_0) = \frac{2}{\pi}\arctan(-\pi\bar{\rho}_0 V_1). \tag{37}$$

For $|\delta_d|$, $\Gamma \ll U \ll D$, one finds that

$$\langle \hat{n}_d - 1\rangle_0 = -\frac{8\delta_d\Gamma}{\pi A_\Lambda U^2}, \tag{38}$$

where A_Λ is defined in Eq. (31).

Even though the stable fixed point of the Anderson model for any $\Gamma>0$ is one of the strong-coupling fixed points described above, the route by which such a fixed point is reached can vary widely, depending on the relative values of U, δ_d, and Γ. For our immediate purposes, it suffices to focus on the symmetric ($\delta_d=0$) model, for which there is a single strong-coupling fixed point corresponding to $V_0=\pm\infty$ or $V_1=0$. If the on-site Coulomb repulsion is strong enough that the system enters the local-moment regime (T, $\Gamma \ll U$), then it is possible to perform a Schrieffer-Wolff transformation[54] that restricts the system to the sector $n_d=1$ and reduces the Anderson model to the Kondo model described by the Hamiltonian

$$\hat{H}_{\rm K} = \hat{H}_{\rm band} + \frac{J_z}{4N_k}(\hat{n}_{d\uparrow} - \hat{n}_{d\downarrow})\sum_{\mathbf{k},\mathbf{k}'}(c_{\mathbf{k}\uparrow}^{\dagger}c_{\mathbf{k}'\uparrow} - c_{\mathbf{k}\downarrow}^{\dagger}c_{\mathbf{k}'\downarrow}) + \frac{J_\perp}{2N_k}\sum_{\mathbf{k},\mathbf{k}'}(d_{\uparrow}^{\dagger}d_{\downarrow}c_{\mathbf{k}\downarrow}^{\dagger}c_{\mathbf{k}'\uparrow} + \mathrm{H.c.}), \tag{39}$$

where

$$\rho_0 J_z = \rho_0 J_\perp = \frac{8\Gamma}{\pi U}. \tag{40}$$

The stable fixed point is approached below an exponentially small Kondo temperature $T_{\rm K}$ when the spin-flip processes associated with the $J_\perp$ term in $\hat{H}_{\rm K}$ cause the effective values of $\rho_0 J_z$ and $\rho_0 J_\perp$ to renormalize to strong coupling, resulting in many-body screening of the impurity spin.

Motivated by the discussion in Sec. III A, we also consider the case of strong on-site Coulomb *attraction*. In the local-charge regime (T, $\Gamma \ll -U$), a canonical transformation similar to the Schrieffer-Wolff transformation restricts the system to the sectors $n_d=0$ and $n_d=2$ and maps the Anderson model onto a charge Kondo model described by the Hamiltonian

$$\hat{H}_{\rm CK} = \hat{H}_{\rm band} + \frac{W_d}{N_k}(\hat{n}_d - 1)\sum_{\mathbf{k},\mathbf{k}'}(c_{\mathbf{k}\uparrow}^{\dagger}c_{\mathbf{k}'\uparrow} + c_{\mathbf{k}\downarrow}^{\dagger}c_{\mathbf{k}'\downarrow} - \delta_{\mathbf{k},\mathbf{k}'}) + \frac{2W_p}{N_k}\sum_{\mathbf{k},\mathbf{k}'}(d_{\uparrow}^{\dagger}d_{\downarrow}^{\dagger}c_{\mathbf{k}\downarrow}c_{\mathbf{k}'\uparrow} + \mathrm{H.c.}), \tag{41}$$

where

$$\rho_0 W_d = \rho_0 W_p = \frac{2\Gamma}{\pi|U|}. \tag{42}$$

In this case, the stable fixed point is approached below an exponentially small (charge) Kondo temperature $T_{\rm K}$ when the charge-transfer processes associated with the W_p term in $\hat{H}_{\rm CK}$ cause the effective values of $\rho_0 W_d$ and $\rho_0 W_p$ to renormalize to strong coupling, resulting in many-body screening of the impurity isospin degree of freedom [associated with the d-operator terms in Eqs. (19)].

Between the opposite extremes of large positive U and large negative U is a mixed-valence regime (T, $|U| \ll \Gamma$) in which interactions play only a minor role. Here, the stable fixed point is approached below a temperature of order Γ

when the effective value of $\sqrt{\Gamma/(2\pi D)}$ scales to strong coupling, signaling strong mixing of the impurity levels with the single-particle states of the conduction band.

C. Expectations for the full model

Insight into the behavior of the full charge-coupled BFA model described by Eqs. (1)–(6) can be gained by performing a Lang-Firsov[55] transformation $\hat{H}_{\mathrm{CCBFA}} \rightarrow \hat{H}'_{\mathrm{CCBFA}} = \hat{U}^{-1}\hat{H}_{\mathrm{CCBFA}}\hat{U}$ with

$$\hat{U} = \exp\left[(\hat{n}_d - 1)\sum_{\mathbf{q}} \frac{\lambda_{\mathbf{q}}}{\sqrt{N_q}\omega_{\mathbf{q}}}(a_{\mathbf{q}} - a_{\mathbf{q}}^{\dagger})\right]. \tag{43}$$

The transformation eliminates $\hat{H}_{\text{imp-bath}}$, leaving

$$\hat{H}'_{\mathrm{CCBFA}} = \hat{H}'_{\mathrm{imp}} + \hat{H}_{\mathrm{band}} + \hat{H}_{\mathrm{bath}} + \hat{H}'_{\text{imp-band}}, \tag{44}$$

where $\hat{H}'_{\mathrm{imp}}$ is as defined in Eqs. (23) and (24), and

$$\hat{H}'_{\text{imp-band}} = \frac{1}{\sqrt{N_k}}\sum_{\mathbf{k},\sigma}\left\{V_{\mathbf{k}} \exp\left[\sum_{\mathbf{q}} \frac{\lambda_{\mathbf{q}}(a_{\mathbf{q}} - a_{\mathbf{q}}^{\dagger})}{\sqrt{N_q}\omega_{\mathbf{q}}}\right] c_{\mathbf{k}\sigma}^{\dagger} d_{\sigma} + V_{\mathbf{k}}^{*} \exp\left[-\sum_{\mathbf{q}} \frac{\lambda_{\mathbf{q}}(a_{\mathbf{q}} - a_{\mathbf{q}}^{\dagger})}{\sqrt{N_q}\omega_{\mathbf{q}}}\right] d_{\sigma}^{\dagger} c_{\mathbf{k}\sigma}\right\}. \tag{45}$$

In addition to renormalizing the impurity interaction from U to U_{eff} entering $\hat{H}'_{\mathrm{imp}}$, the e-b coupling causes every hybridization event to be accompanied by the creation and annihilation of arbitrarily large numbers of bosons.

In the case of the Anderson-Holstein model [Eq. (10)], various limiting behaviors are understood.[18] In the *instantaneous limit* $\omega_0 \gg \Gamma$, the bosons adjust rapidly to any change in the impurity occupancy; for $\lambda_0^2/\omega_0 \ll U \ll \omega_0$, the physics is essentially that of the Anderson model with $U \rightarrow U_{\mathrm{eff}}$, while for $\lambda_0^2/\omega_0 \gg D, U, \Gamma$, there is also a reduction from Γ to $\Gamma \exp[-(\lambda_0/\omega_0)^2]$ in the rate of scattering between the $n_d=0$ and $n_d=2$ sectors, reflecting the reduced overlap between the ground states in these two sectors. In the *adiabatic limit* $\omega_0 \ll \Gamma$, the phonons are unable to adjust on the typical time scale of hybridization events, and neither U nor Γ undergoes significant renormalization.

Similar analysis for the charge-coupled BFA model is complicated by the presence of a continuum of bosonic mode energies ω, only some of which fall in the instantaneous or adiabatic limits. Nonetheless, we can use results for the cases $\Gamma = 0$ (Sec. III A) and $\lambda = 0$ (Sec. III B), as well as those for the Anderson-Holstein model, to identify likely behaviors of the full model. Specifically, we focus here on the evolution with decreasing temperature of the effective Hamiltonian describing the essential physics of the symmetric ($\epsilon_d = -U/2$) model at the current temperature. This effective Hamiltonian is obtained under the assumption that real excitations of energy above the ground state $E \geqslant \eta T$—where η is a number around 5, say—make a negligible contribution to the observable properties, and thus can be integrated from the problem.

Based on the preceding discussion, one expects that at high temperatures $T \gg \Gamma$, the physics of the charge-coupled BFA model will be very similar to that of the Anderson model with U replaced by $\tilde{U}(\eta T)$, where

$$\tilde{U}(E) = U - \frac{2}{\pi}\int_{E}^{\infty} \frac{B(\omega)}{\omega} d\omega. \tag{46}$$

Note that $\tilde{U}(0)$ is identical to U_{eff} defined in Eq. (24). For the bath spectral density in Eq. (8) with $s > 0$,

$$\tilde{U}(E) = U - \frac{2(K_0\lambda)^2}{\pi s}[1 - (E/\Omega)^s]\Omega. \tag{47}$$

When analyzing NRG data, we instead use

$$\tilde{U}^{\mathrm{NRG}}(E) = U\{1 - (\lambda/\lambda_{c0})^2[1 - (E/\Omega)^s]\}, \tag{48}$$

where λ_{c0} is the empirically determined value discussed in connection with Eq. (33).

If, upon decreasing the temperature to some value T_{LM}, the system comes to satisfy $\tilde{U}(\eta T_{\mathrm{LM}}) = \eta \max(T_{\mathrm{LM}}, \Gamma)$, then it should enter a local-moment regime described by the effective Hamiltonian $\hat{H}_{\mathrm{LM}} = \hat{H}_{\mathrm{K}} + \hat{H}_{\mathrm{bath}}$ with the exchange couplings in $\hat{H}_{\mathrm{K}}$ [Eq. (39)] determined by Eq. (40) with $U \rightarrow \tilde{U}(\eta T_{\mathrm{LM}})$, similar to what is found in the Anderson-Holstein model.[8] Since they couple only to the high-energy sectors $n_d=0$ and $n_d=2$ that are projected out during the Schrieffer-Wolff transformation, the bosons should play little further role in determining the low-energy impurity physics. The outcome should be a conventional Kondo effect where the e-b coupling contributes only to a renormalization of the Kondo scale T_{K}.

If, instead, at some $T = T_{\mathrm{LC}}$ the system satisfies $\tilde{U}(\eta T_{\mathrm{LC}}) = -\eta \max(T_{\mathrm{LC}}, \Gamma)$, then it should enter a local-charge regime described by the effective Hamiltonian

$$\hat{H}_{\mathrm{LC}} = \hat{H}_{\mathrm{CK}} + \hat{H}_{\mathrm{bath}} + \hat{H}_{\text{imp-bath}}. \tag{49}$$

Based on the behavior of the Anderson-Holstein model,[8] one expects W_d in $\hat{H}_{\mathrm{CK}}$ [Eq. (41)] to be determined by Eq. (42) with $U \rightarrow \tilde{U}(\eta T_{\mathrm{LC}})$ but with W_p exponentially depressed due to the aforementioned reduction in the overlap between the ground states of the $n_d=0$ and $n_d=2$ sectors. The bosons couple to the low-energy sector of the impurity Fock space, so they have the potential to significantly affect the renormalization of W_d and W_p upon further reduction in the temperature. In particular, the λ term in $\hat{H}_{\mathrm{LC}}$, which favors localization of the impurity in a state of well-defined $n_d=0$ or 2, directly competes with the W_p double-charge transfer term that is responsible for the charge Kondo effect of the negative-U Anderson model. This nontrivial competition gives rise to the possibility of a QPT between qualitatively distinct ground states of the charge-coupled BFA model.

Between these extremes, the system can enter a mixed-valence regime of small effective on-site interaction. In this regime, one must retain all the impurity degrees of freedom of the charged-coupled BFA model. The impurity-band hybridization competes with the e-b coupling for control of the impurity, again suggesting the possibility of a QPT.

Each of the regimes discussed above features competition between band-mediated tunneling within the manifold of impurity states and the localizing effect of the bosonic bath. Although the tunneling is dominated by a different process in

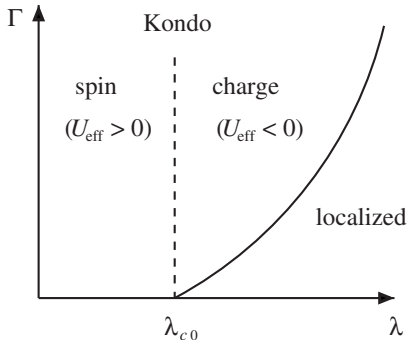

FIG. 3. Schematic phase diagram of the symmetric charge-coupled BFA model for bath exponents $0<s<1$. The solid curve marks the boundary between the Kondo phase, in which the impurity degrees of freedom are screened by conduction electrons, and the localized phase, in which the impurity dynamics are controlled by the coupling to the dissipative bath. The dashed vertical line represents a crossover from a regime in which Kondo screening takes place primarily in the spin sector to a regime in which a charge-Kondo effect is predominant.

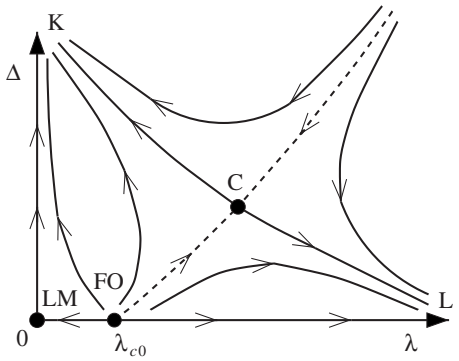

FIG. 4. Schematic renormalization-group flows on the λ-Δ plane for the symmetric charge-coupled BFA model with a bath exponent $0<s<1$. Trajectories with arrows represent the flow of the couplings λ entering Eq. (15) and Δ defined in Eq. (50) under decrease of the high-energy cutoffs on the conduction band and the bosonic bath. Between the basins of attraction of the Kondo fixed point (K) and the localized fixed point (L) lies a separatrix, along which the flow is away from the free-orbital fixed point (FO) located at $\lambda=\lambda_{c0}$, $\Delta=0$ and toward the critical fixed point (C). For $\Delta=0$ only, there is flow from FO toward the local-moment fixed point (LM) at $\lambda=0$.

the three regimes, it always drives the system toward a nondegenerate impurity ground state, whereas the *e-b* coupling favors a doubly-degenerate ($n_d=0,2$) impurity ground state. In order to provide a unified picture of the three regimes (and the regions of the parameter space that lie in between them), we will find it useful to interpret our NRG result in terms of an overall tunneling rate Δ, which has a bare value

$$\Delta \simeq \sqrt{J_\perp^2 + 2\Gamma D/\pi + 16W_p^2}. \tag{50}$$

Here, W_p is assumed to be negligibly small in the local-moment regime, and $J_\perp$ to be similarly negligible in the local-charge regime. If Δ renormalizes to large values while the *e-b* coupling λ scales to weak coupling, then one expects to recover the strong-coupling physics of the Anderson model. If, on the other hand, λ becomes strong while Δ becomes weak, the system should enter a low-energy regime in which the bath governs the asymptotic low-energy long-time impurity dynamics. Whether or not each of these scenarios is realized in practice, and whether or not there are any other possible ground states of the model, can be determined only by more detailed study. These questions are answered by the NRG results reported in the sections that follow.

IV. RESULTS: SYMMETRIC MODEL WITH SUB-OHMIC DISSIPATION

This section presents results for Hamiltonian (1) with $U=-2\epsilon_d>0$ and with sub-Ohmic dissipation characterized by an exponent $0<s<1$. Figure 3 shows a schematic phase diagram on the λ-Γ plane at fixed U. There are two stable phases: the *localized* phase, in which the impurity dynamics are controlled by the coupling to the bosonic bath and the system has a pair of ground states related to one another by a particle-hole transformation, and the *Kondo* phase, in which there is a nondegenerate ground state. These phases are separated by a continuous QPT that takes place on the phase boundary (solid line in Fig. 3), which we parametrize as $\lambda=\lambda_c(\Gamma)$. Within the Kondo phase, the nature of the correlations evolves continuously with increasing λ (at fixed Γ) from a pure spin-Kondo effect for $\lambda=0$ to a predominantly charge-Kondo effect beyond a crossover (dashed line in Fig. 3) associated with the change in sign of $U_{\rm eff}$ defined in Eq. (24).

As s decreases, and the *e-b* coupling becomes increasingly relevant—in a renormalization-group sense [see Eq. (28)]—the phase boundary moves to the left as the localized phase grows at the expense of the Kondo phase, which disappears entirely for $s\leqslant 0$. As will be seen in Sec. V, the phase diagram of the Ohmic ($s=1$) problem has the same topology as Fig. 3, even though (as described in Sec. V) the nature of the QPT is qualitatively different than for $0<s<1$. For $s>1$, the *e-b* coupling is irrelevant, and the system is in the Kondo phase for all $\Gamma>0$.

The remainder of this section presents the evidence for the preceding statements. We first discuss the renormalization-group flows and fixed points. We then turn to the behavior in the vicinity of the phase boundary, focusing in particular on the critical response of the impurity charge to a local electric potential. Following that, we present results for the impurity spectral function and show that the low-energy scale extracted from this spectral function supports the qualitative picture laid out in the paragraphs above and summarized in Fig. 3.

A. NRG flows and fixed points

Figure 4 plots the schematic renormalization-group flows of the couplings λ entering Eq. (15) and Δ defined in Eq. (50) for a symmetric impurity ($U=-2\epsilon_d$) coupled to a bath described by an exponent $0<s<1$. These flows are deduced from the evolution of the many-body spectrum with increasing iteration number N, i.e., with reduction in the effective

band and bath cutoffs $\tilde{D}=\tilde{\Omega}\simeq D\Lambda^{-N/2}$. A separatrix (dashed line) forms the boundary between the basins of attraction of a pair of stable fixed points, regions that correspond to the two phases shown in Fig. 3. Figure 4 also shows three unstable fixed points. In contrast to the situation at other points on the flow diagram, each of the fixed points exhibits a many-body spectrum that can be interpreted as the direct product of a set of bosonic excitations and a set of fermionic excitations.

The *Kondo* fixed point corresponds in the renormalization-group language of Fig. 4 to effective couplings $\lambda=0$ and $\Delta=\infty$. The many-body spectrum decomposes into the direct product of (i) the excitations of a free bosonic chain described by Eq. (13) alone, and (ii) the strong-coupling excitations of the Kondo (or symmetric Anderson) model, corresponding to free electrons with a Fermi-level phase shift of $\pi/2$. This spectrum, which exhibits SU(2) symmetry both in the spin and charge (isospin) sectors, is identical to that found throughout the Kondo phase of the particle-hole-symmetric Ising BFK Hamiltonian[38,39] (a model in which the bosons couple to the impurity's spin rather than its charge).

The schematic RG flow diagram in Fig. 4 shows a *localized* fixed point corresponding to $\lambda=\infty$ and $\Delta=0$. However, this is really a *line* of fixed points described by $\hat{H}_{\rm LC}$ [Eq. (49)] with effective couplings $\lambda=\infty$, $W_p=0$, and $0\leqslant W_d<\infty$. Since $W_p=0$, the impurity occupancy takes a fixed value $n_d=0$ or 2. (It is important to distinguish n_d, used to characterize the fixed-point excitations, from the physical expectation value of $\hat{n}_d$. The latter quantity is discussed in Sec. IV E 1.)

Each fixed point along the localized line has an excitation spectrum that decomposes into the direct product of (i) bosonic excitations identical to those at the localized fixed point of the spin-boson model[29] with the same bath exponent s, and (ii) fermionic excitations described by a Hamiltonian

$$\hat{H}_{L,f}^{\rm NRG}=\hat{H}_{\rm band}^{\rm NRG}+W_d(n_d-1)\left(\sum_\sigma f_{0\sigma}^\dagger f_{0\sigma}-1\right), \qquad (51)$$

which is just the discretized version of $\hat{H}_{\rm CK}$ [Eq. (41)] with $W_p=0$ and the operator $\hat{n}_d$ replaced by the parameter n_d. The low-lying many-body eigenstates of $\hat{H}_{L,f}^{\rm NRG}$ appear in degenerate pairs, one member of each pair corresponding to $n_d=0$ and the other to $n_d=2$. The fixed-point coupling W_d increases monotonically as the bare e-b coupling λ decreases from infinity and diverges on approach to the phase boundary. As illustrated in Fig. 5, this divergence can be fitted to the power-law form

$$W_d\propto(\lambda-\lambda_c)^{-\beta}\quad\text{for }\lambda\to\lambda_c^+. \qquad (52)$$

For reasons that will be explained in Sec. IV E 1, the numerical value of β coincides, to within a small error, with that of the order-parameter exponent β defined in Eq. (71).

The *free-orbital* fixed point $(\lambda=\lambda_{c0},\Delta=0)$ is unstable with respect to a bare $\Gamma\neq0$ or any deviation of λ from $\lambda_{c0}\equiv\lim_{\Gamma\to0}\lambda_c(\Gamma)$. The *local-moment* fixed point $(\lambda=\Delta=0)$, at which the impurity has a spin-$\frac{1}{2}$ degree of freedom decoupled from the band and from the bath, is reached only for bare couplings $\Gamma=0$ (hence, $\Delta=0$) and $\lambda<\lambda_{c0}$.

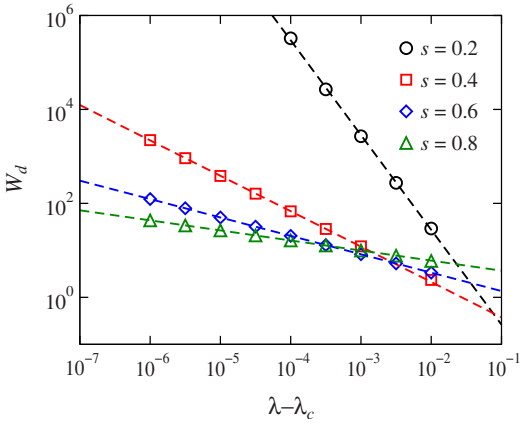

FIG. 5. (Color online) Fixed-point coupling W_d entering Eq. (51) vs e-b coupling $\lambda-\lambda_c$ in the localized phase near the phase boundary at $\lambda=\lambda_c$. Results are shown for $U=-2\epsilon_d=0.1$, $\Lambda=9$, $N_s=500$, $N_b=8$, four different values of the bath exponent s, and $\Gamma=0.5$, 1.0, 10, and 50 for $s=0.2$, 0.4, 0.6, and 0.8, respectively (Ref. 56). The power-law divergence of W_d as $\lambda\to\lambda_c^+$ [Eq. (52)] is reflected in the linear behaviors of data on a logarithmic scale. The numerical values of the exponent β obtained here are identical (to within small errors) to those listed in Table III.

Of greatest interest is the unstable *critical* fixed point that is reached for any bare couplings lying on the boundary $\lambda=\lambda_c(\Gamma)$ between the Kondo and localized phases. At this fixed point, the low-lying spectrum can be constructed as the direct product of (i) the critical spectrum of the spin-boson model with the same bath exponent s, and (ii) the strong-coupling spectrum of the Kondo (or symmetric Anderson) model. This spectrum, which exhibits full SU(2) symmetry in both the spin and isospin sectors, is identical to that at the critical point of the Ising-anisotropic Bose-Fermi Kondo model[57] and is illustrated in Fig. 3(c) of Ref. 39.

The decomposition of the critical spectrum can be understood by considering the flow of couplings entering the local-charge Hamiltonian $\hat{H}_{\rm LC}$ defined in Eq. (49). The fixed-point value of the density-density coupling is $W_d=\infty$ in the charge-Kondo regime of the Kondo phase and diverges according to Eq. (52) in the localized phase. It is therefore reasonable to assume that in the vicinity of the phase boundary, W_d rapidly renormalizes to strong coupling, locking the impurity site and site $n=0$ of the fermionic chain into one of just two states, which we can write in a pseudospin notation as $|\Uparrow\rangle=d_\uparrow^\dagger d_\downarrow^\dagger|0\rangle$ and $|\Downarrow\rangle=f_{0\uparrow}^\dagger f_{0\downarrow}^\dagger|0\rangle$, where $|0\rangle$ is the no-particle vacuum. Hopping of electrons on or off site $n=0$ is forbidden, so the discretized form of $\hat{H}_{\rm LC}$ reduces to an effective Hamiltonian

$$\hat{H}_{\rm LC}^{\rm NRG}(W_d=\infty)=\hat{H}_{\rm SC}^{\rm NRG}(0)+\hat{H}_{\rm SBM}^{\rm NRG}. \qquad (53)$$

Here, $\hat{H}_{\rm SC}^{\rm NRG}(0)$ [Eq. (34)] acts only on fermionic chain sites $n\geqslant1$ and yields the Kondo/Anderson strong-coupling excitation spectrum, while

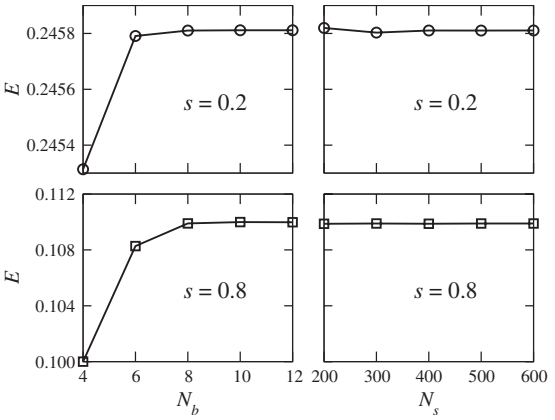

FIG. 6. Dependence of the energy of the first bosonic excitation at the critical point ($\lambda=\lambda_c$) on the NRG truncation parameters N_b and N_s. Results are shown for $U=-2\epsilon_d=0.1$, $\Gamma=0.01$, $\Lambda=9$, and bath exponents $s=0.2$ and $s=0.8$. In the left panels, $N_s=500$, while in the right panels $N_b=8$.

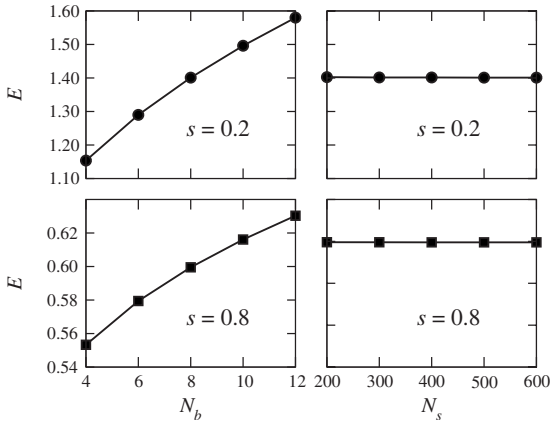

FIG. 7. Dependence of the energy of the first bosonic excitation in the localized phase ($\lambda=1.1\lambda_c$) on the NRG truncation parameters N_b and N_s. All other parameters are as in Fig. 6.

$$\hat{H}_{\rm SBM}^{\rm NRG}=\hat{H}_{\rm bath}^{\rm NRG}+2W_p(|\Uparrow\rangle\langle\Downarrow|+|\Downarrow\rangle\langle\Uparrow|)+\frac{\Omega K_0\lambda}{\sqrt{\pi(s+1)}}(|\Uparrow\rangle\langle\Uparrow|-|\Downarrow\rangle\langle\Downarrow|)(b_0+b_0^\dagger) \quad (54)$$

acts on the remaining degrees of freedom in the problem in a subspace of states all carrying quantum numbers $S=S_z=Q=0$. $\hat{H}_{\rm SBM}^{\rm NRG}$ is precisely the discretized form of the spin-boson Hamiltonian with tunneling rate $\Delta=4W_p$ and dissipation strength $\alpha=2(K_0\lambda)^2/\pi$. These two couplings compete with one another, with three possible outcomes: (1) Δ can scale to infinity and α to zero, resulting in flow to the delocalized fixed point (the Kondo fixed point of the charge-coupled BFA model); (2) α can scale to infinity and Δ to zero, yielding flow to the localized fixed point; or (3) both couplings can renormalize to finite values $\Delta=\Delta_C$, $\alpha=\alpha_C$ at the critical point. This picture implies that the universal critical behavior of the charge-coupled BFA model should be identical to that of the spin-boson model, the conduction-band electrons serving only to dress the $n_d=0,2$ impurity levels and to renormalize the impurity tunneling rate and the dissipation strength.

Given that the NRG approach necessarily involves Fock-space truncation, it is instructive to examine the dependence of the fixed-point spectra on the parameters N_s and N_b denoting, respectively, the number of states retained from one NRG iteration to the next and the maximum number of bosons allowed per site of the bosonic chain. Figure 6 shows, for representative bath exponents $s=0.2$ and $s=0.8$, that the energy of the lowest bosonic excitation at $\lambda=\lambda_c$ converges rapidly with increasing N_s and N_b. This behavior suggests that for $\Lambda=9$, at least, $N_s=500$, and $N_b=8$ are sufficient for studying the physics at the critical point.

By contrast, the lowest bosonic excitation energy for $\lambda=1.1\lambda_c$, plotted in Fig. 7, converges only slowly with respect to N_b. This points to the failure of the truncated bosonic basis deep inside the localized phase of the sub-Ohmic model, where the mean boson number per site is expected to diverge according to Eq. (27). This interpretation is confirmed by calculation of the expectation value of the total boson number,

$$\hat{B}_N=\sum_m^{M(N)} b_m^\dagger b_m, \quad (55)$$

where $M(N)$ denotes the highest labeled bosonic site present at iteration N. Our results for $\langle\hat{B}_{20}\rangle$ vs N_b (not shown) are very similar to those in Fig. 8 of Ref. 39, with convergence by $N_b=8$ at the critical point, but no evidence of such convergence for an e-b coupling 10% over the critical value.

Recently, Bulla *et al.* applied a "star" reformulation of the NRG to the spin-boson model.[29] While this approach provides a good description of the localized fixed point, it does not correctly capture the physics of the delocalized phase (corresponding to the Kondo phase of the present model) or of the critical point that separates the two stable phases. For this reason, we prefer to work with the "chain" formulation summarized in Sec. II.

B. Critical coupling

Figure 8 plots the critical e-b coupling $\lambda_c(\Gamma)$ for fixed $U=-2\epsilon_d$ and four different values of the bath exponent s. As expected, with increasing Γ, the critical coupling increases smoothly from $\lambda_c(\Gamma=0)\equiv\lambda_{c0}$, reflecting the fact that entry to the localized phase requires an e-b coupling sufficiently large not only to drive $U_{\rm eff}$ negative but also to overcome the reduction in the electronic energy that derives from the hybridization. We believe that the vertical slope of the $s=0.2$ phase boundary as it approaches the horizontal axis in Fig. 8 is an artifact stemming from the same source as the NRG overestimate of λ_{c0} for the same bath exponent. (See the discussion of Fig. 2 in Sec. III A.)

In the sections that follow, we show that the critical properties of the charge-coupled BFA model map, under interchange of spin and charge degrees of freedom, onto those of the spin-coupled BFA model studied (along with the corre-

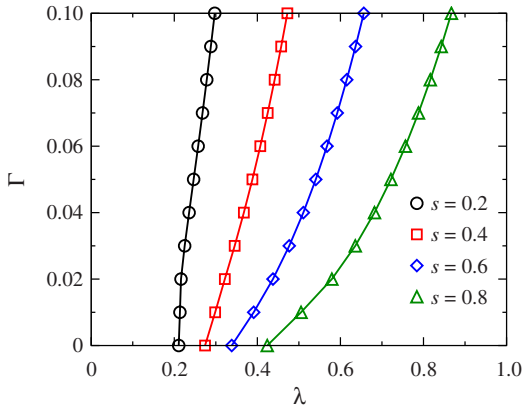

FIG. 8. (Color online) Critical coupling λ_c vs hybridization width Γ for $U=-2\epsilon_d=0.1$, $\Lambda=9$, $N_s=500$, $N_b=8$, and the bath exponents s listed in the legend.

sponding Ising BFK model) in Ref. 39. The spin-coupled model is described by Eqs. (1)–(5) and (12)–(14), with Eqs. (6) and (15) replaced by

$$\hat{H}_{\text{imp-bath}} = \frac{1}{2\sqrt{N_q}}(\hat{n}_{d\uparrow} - \hat{n}_{d\downarrow})\sum_{\mathbf{q}} g_{\mathbf{q}}(a_{\mathbf{q}} + a_{-\mathbf{q}}^{\dagger}) \tag{56}$$

and

$$\hat{H}_{\text{imp-bath}}^{\text{NRG}} = \frac{\Omega K_0 g}{2\sqrt{\pi(s+1)}}(\hat{n}_{d\uparrow} - \hat{n}_{d\downarrow})(b_0 + b_0^{\dagger}). \tag{57}$$

In light of the parallels between the universal critical behavior of the two models, it is of interest to compare their critical couplings, making due allowance for the additional prefactor of $\frac{1}{2}$ that enters Eqs. (56) and (57).

Figure 9 plots the s dependence of λ_c and $g_c/2$ for fixed values of $U=-2\epsilon_d$ and Γ. For all $0<s\leqslant 1$, λ_c is found to exceed $g_c/2$. This fact can be understood by noting the contrasting role of the e-b coupling in the two models. In the spin-coupled BFA model, increasing g from zero immediately begins to localize the impurity in a state of fixed S_z and thereby to impede the spin-flip processes that are central to the Kondo effect. In the charge-coupled model, by contrast,

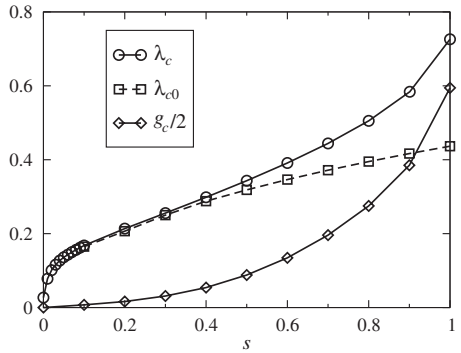

FIG. 9. Variation with bath exponent s of the critical couplings λ_c and λ_{c0} in the charge-coupled BFA model (this work) and $g_c/2$ in the spin-coupled BFA model (Ref. 39). Results are shown for $U=-2\epsilon_d=0.1$, $\Gamma=0.01$, $\Lambda=9$, $N_s=500$, and $N_b=8$.

increasing λ from zero initially acts to decrease the effective Coulomb repulsion and hence to enhance charge fluctuations on the impurity site; only for $\lambda_c \gtrsim \lambda_{c0}$ do further increases in the e-b coupling serve to localize the impurity in a state of fixed charge, eventually leading to the suppression of the charge Kondo effect at $\lambda=\lambda_c$.

C. Crossover scale

Under the renormalization-group flows sketched in Fig. 4, the system passes, with decreasing energy cutoff or decreasing temperature, between the regions of influence of different renormalization-group fixed points. For bare parameters that place the system near the boundary between the Kondo and localized phases, the free-orbital fixed point typically governs the behavior at temperatures much greater than the Kondo temperature T_K of the Anderson model obtained by setting $\lambda = 0$ in Eq. (1). For temperatures between of order T_K and a crossover scale T_*, the system exhibits quantum critical behavior controlled by thermal fluctuations about the unstable critical point. Finally, the physics in the regime $T \lesssim T_*$ is governed by one or other of the two stable fixed points: Kondo or localized.

For fixed values of all other parameters, one expects T_* to vanish as the e-b coupling approaches its critical value according to a power law,

$$T_* \propto |\lambda - \lambda_c|^{\nu} \quad \text{for } \lambda \to \lambda_c, \tag{58}$$

where ν is the correlation-length exponent.[4] The crossover scale can be determined directly from the NRG solution via the condition $T_* \propto \Lambda^{-N_*/2}$, where N_* is the number of the iteration at which the many-body energy levels cross over to those of a stable fixed point. There is some arbitrariness as to what precisely constitutes crossover of the levels. Different criteria will produce $T_*(\lambda)$ values that differ from one another by a λ-independent multiplicative factor. It is of little importance what definition of N_* one uses, provided that it is applied consistently.

Figure 10 shows typical dependences of T_* on $\lambda_c-\lambda$ in the Kondo phase. Equation (58) holds very well over several decades, as demonstrated by the linear behavior of the data on a log-log plot. We find that the numerical values of $\nu(s)$, some of which are listed in Table II, are identical (within small errors), to those of the spin-boson and Ising BFK models for the same bath exponent s. This supports the notion that the critical point of the charge-coupled BFA model belongs to the same universality class as the critical points of the spin-boson and Ising BFK models. However, to confirm this equivalence, we must compare other critical exponents, as reported below.

D. Thermodynamic susceptibilities

In this section, we consider the response of the charge-coupled BFA model to a global magnetic field H and to a global electric potential Φ. These external probes enter the Hamiltonian through an additional term

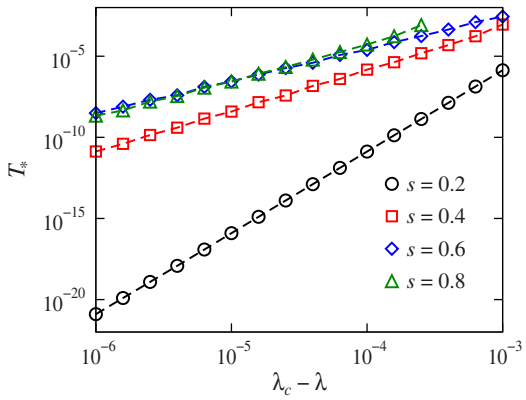

FIG. 10. (Color online) Crossover scale T_* vs $\lambda_c - \lambda$ on the Kondo side of the critical point for four different values of the bath exponent s, with all other parameters as in Fig. 5. The slope of each line on this log-log plot gives the correlation-length exponent $\nu(s)$ defined in Eq. (58).

$$\hat{H}_{\rm ext} = HS_z + \Phi Q, \tag{59}$$

where S_z and Q are defined in Eqs. (16) and (18), respectively. In particular, we focus on the static impurity spin susceptibility $\chi_{s,\rm imp} = -\partial^2 F_{\rm imp}/\partial H^2$ and the static impurity charge susceptibility $\chi_{c,\rm imp} = \partial^2 F_{\rm imp}/\partial \Phi^2$. Here, $F_{\rm imp} = \Delta(F)$, where $\Delta(X)$ is the difference between (i) the value of the bulk property X when the impurity is present and (ii) the value of X when the impurity is removed from the system. It is straightforward to show that

$$T\chi_{s,\rm imp} = \Delta(\langle\langle \hat{S}_z^2 \rangle\rangle - \langle\langle \hat{S}_z \rangle\rangle^2), \tag{60}$$

$$T\chi_{c,\rm imp} = \Delta(\langle\langle \hat{Q}^2 \rangle\rangle - \langle\langle \hat{Q} \rangle\rangle^2), \tag{61}$$

where, for any operator $\hat{A}$,

$$\langle\langle \hat{A} \rangle\rangle = \frac{{\rm Tr}\, \hat{A} \exp(-\hat{H}/T)}{{\rm Tr} \exp(-\hat{H}/T)}. \tag{62}$$

Note that with the above definitions, $\lim_{T\to\infty} T\chi_{s,\rm imp} = \frac{1}{8}$ but $\lim_{T\to\infty} T\chi_{c,\rm imp} = \frac{1}{2}$, a factor of four difference that must be taken into account when comparing the two susceptibilities. Since each $T\chi_{\rm imp}$ is calculated as the difference of bulk quantities, its evaluation using the NRG method is complicated by significant discretization and truncation errors. In order to obtain reasonably well-converged results for $T\chi_{\rm imp}$, we retain $N_s = 2000$ states after each NRG iteration. However, even this number is insufficient to allow reliable extraction of $\chi_{\rm imp} \equiv (T\chi_{\rm imp})/T$ as $T \to 0$.

TABLE II. Correlation-length critical exponent ν vs bath exponent s for the charge-coupled Bose-Fermi Anderson model (CC-BFA, this work) and for the Ising-anisotropic Bose-Fermi Kondo model (BFK, from Refs. 38 and 39). Parentheses surround the estimated nonsystematic error in the last digit.

s	0.2	0.4	0.6	0.8
ν(CC-BFA)	4.99(3)	2.52(2)	1.97(4)	2.12(6)
ν(BFK)	4.99(5)	2.50(1)	1.98(3)	2.11(2)

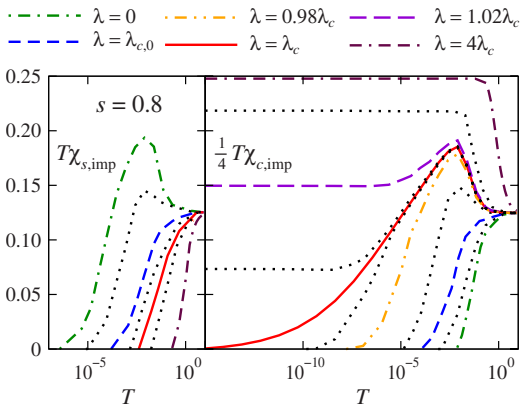

FIG. 11. (Color online) Temperature dependence of the impurity contribution to the static spin (left) and charge (right) susceptibilities for $s=0.8$, $U=-2\epsilon_d=0.1$, $\Gamma=0.01$, $\Lambda=9$, $N_s=2000$, $N_b=8$, and different values of the e-b coupling λ. Dotted curves correspond to e-b couplings lying between the λ values specified in the legend for the adjacent nondotted curves. For $\lambda=\lambda_{c0}\simeq 0.396$, the spin and charge susceptibilities are equivalent: $\chi_{s,\rm imp}(T) \simeq \frac{1}{4}\chi_{c,\rm imp}(T)$. For $\lambda < \lambda_{c0}$, the spin response is stronger, while for $\lambda > \lambda_{c0}$, the charge response dominates. For $\lambda \leqslant \lambda_c \simeq 0.505\,218\,1$, $\lim_{T\to 0} T\chi_{c,\rm imp}(T) = 0$, whereas for $\lambda > \lambda_c$, the limiting value is nonzero and obeys Eqs. (65) and (66).

Figure 11 plots NRG results for $T\chi_{s,\rm imp}(T)$ and $\frac{1}{4}T\chi_{c,\rm imp}(T)$, calculated for bath exponent $s=0.8$ and different values of the e-b coupling λ. For $\lambda \ll \lambda_{c0}$ (see Sec. III A), both impurity susceptibilities behave very much as they do in the Anderson model: with decreasing temperature, $T\chi_{c,\rm imp}$ quickly falls toward zero, signaling quenching of charge fluctuations upon entry into the local-moment regime, whereas $T\chi_{s,\rm imp}$ initially rises toward its local-moment value of $\frac{1}{4}$, before dropping to zero for $T \ll T_*$ on approach to the Kondo fixed point. With increasing λ, the charge response grows and the spin response is suppressed. The two susceptibilities are approximately equivalent for $\lambda=\lambda_{c0}$, where the effective Coulomb interaction $U_{\rm eff}=0$. For still stronger e-b couplings, $T\chi_{s,\rm imp}$ plunges rapidly as the temperature is decreased, whereas $T\chi_{c,\rm imp}$ first rises on entry to the local-charge regime before dropping to satisfy

$$\lim_{T\to 0} T\chi_{c,\rm imp}(T) = 0 \quad \text{for } \lambda < \lambda_c. \tag{63}$$

These trends are very similar to those exhibited[10] by the Anderson-Holstein model. In that model, however, the drop in $T\chi_{c,\rm imp}(T)$ takes place[8] for strong e-b couplings $\lambda_0 \gg \sqrt{\omega_0 U/2}$ around an effective Kondo temperature $T_K^{\rm eff} \sim D\exp(-\pi\lambda_0^4/\Gamma\omega_0^3)$. In the charge-coupled BFA model, by contrast, neither the spin susceptibility nor the charge susceptibility exhibits any obvious feature that correlates with the vanishing of T_* as $\lambda \to \lambda_c^-$. This can be understood by noting that the impurity susceptibilities are determined purely by the fermionic part of the excitation spectrum, whose asymptotic low-energy form is the same at the critical fixed point (which governs the behavior in the quantum criti-

cal regime $T_* \lesssim T \lesssim T_K$) as at the Kondo fixed point (which controls the regime $T \lesssim T_*$).

The behavior of the static impurity spin susceptibility is qualitatively unchanged upon crossing from the Kondo phase to the localized phase. However, for $\lambda > \lambda_c$, $T\chi_{c,\mathrm{imp}}$ approaches at low temperatures a nonzero value that can be inferred from the effective Hamiltonian $\hat{H}_{L,f}^{\mathrm{NRG}}$ [Eq. (51)]. Electrons near the Fermi level experience an s-wave phase shift,

$$\delta(\omega = 0) = \begin{cases} \delta_0 & \text{for } n_d = 0 \\ \pi - \delta_0 & \text{for } n_d = 2, \end{cases} \tag{64}$$

where n_d labels the two disconnected sectors of $\hat{H}_{L,f}^{\mathrm{NRG}}$, and

$$\delta_0 = \arctan(\pi \bar{\rho}_0 W_d), \quad 0 \leqslant \delta_0 \leqslant \pi/2, \tag{65}$$

with $\bar{\rho}_0$ being the effective conduction-band density of states defined in Eq. (30). It is then straightforward to show that

$$\lim_{T \to 0} T\chi_{c,\mathrm{imp}}(T) = (1 - 2\delta_0/\pi)^2. \tag{66}$$

Equations (52), (65), and (66) together imply that

$$\lim_{T \to 0} T\chi_{c,\mathrm{imp}}(T) \propto (\lambda - \lambda_c)^{2\beta} \quad \text{for } \lambda \to \lambda_c^+. \tag{67}$$

As this example illustrates, the thermodynamic susceptibilities contain signatures of an evolution from a spin-Kondo effect to a charge-Kondo effect. Furthermore, Eqs. (63) and (67) suggest that $\chi_{c,\mathrm{imp}}$ may serve as the order-parameter susceptibility for the QPT. However, neither susceptibility manifests the vanishing of the crossover scale T_* on approach to the transition from the Kondo side. Moreover, the conservation of Q prevents $\chi_{c,\mathrm{imp}}$ from acquiring an anomalous temperature dependence in the quantum-critical regime.[58] Thus, one is led to conclude that the response to a global electric potential Φ does not provide access to the critical fluctuations near the QPT.

E. Local charge response

Given the nature of the coupling in Hamiltonian (1) between the impurity and the bosonic bath, we expect to be able to probe the quantum critical point through the system's response to a local electric potential ϕ that acts solely on the impurity charge, entering the Hamiltonian via an additional term

$$\hat{H}_{c,\mathrm{loc}} = \phi(\hat{n}_d - 1). \tag{68}$$

A nonzero ϕ is equivalent to a shift in δ_d entering Eq. (9) away from its bare value $\epsilon_d + U/2 = 0$.

In this section we show that for sub-Ohmic bath exponents $0 < s < 1$, (i) the response to a static ϕ is described by critical exponents that satisfy hyperscaling relations characteristic of an interacting quantum critical point, (ii) numerical values of these critical exponents are identical to those of the spin-boson and Ising BFK models, and (iii) the dynamical response is consistent with the presence of ω/T scaling in the vicinity of the quantum critical point.

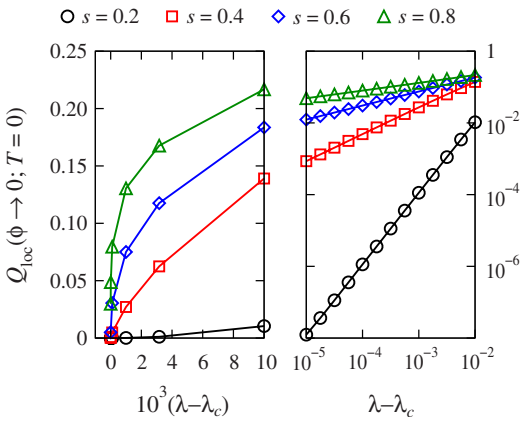

FIG. 12. (Color online) Impurity charge $\lim_{\phi \to 0^-} Q_{\mathrm{loc}}(\lambda, \phi; T = 0)$ vs e-b coupling $\lambda - \lambda_c$ for four different values of the bath exponent s. All other parameters are as in Fig. 5. As λ approaches λ_c from above, $\lim_{\phi \to 0^-} Q_{\mathrm{loc}}(\lambda, \phi; T = 0)$ vanishes (left panel) in a power-law fashion (right panel) described by Eq. (71).

1. Static local charge response

The response to imposition of a static local potential ϕ is measured by the thermodynamic average value of the impurity charge,

$$Q_{\mathrm{loc}} = \langle\langle \hat{n}_d - 1 \rangle\rangle, \tag{69}$$

and through the static local charge susceptibility

$$\chi_{c,\mathrm{loc}}(T; \omega = 0) = -\left.\frac{\partial Q_{\mathrm{loc}}}{\partial \phi}\right|_{\phi = 0} = -\lim_{\phi \to 0} \frac{Q_{\mathrm{loc}}}{\phi}. \tag{70}$$

In NRG calculations of $\lim_{\phi \to 0} Q_{\mathrm{loc}}(\phi)$ and $\chi_{c,\mathrm{loc}}$, we use potentials in the range $10^{-13} \leqslant |\phi| \leqslant 10^{-10}$.

As illustrated in Fig. 12, the "spontaneous impurity charge" $\lim_{\phi \to 0} Q_{\mathrm{loc}}(\lambda, \phi; T = 0)$ indeed serves as an order parameter for the QPT between the Kondo and localized phases. This quantity vanishes for all $\lambda < \lambda_c$ and is nonzero for $\lambda > \lambda_c$, its onset being described by the power law

$$\lim_{\phi \to 0} Q_{\mathrm{loc}}(\lambda, \phi; T = 0) \propto (\lambda - \lambda_c)^{\beta} \quad \text{for } \lambda \to \lambda_c^+. \tag{71}$$

In the localized phase, the presence of an infinitesimal local potential restricts the effective Hamiltonian (51) to just one n_d sector: $n_d = 0$ for $\phi > 0$ or $n_d = 2$ for $\phi < 0$. Then substituting Eq. (64) into the Friedel sum rule $\langle \hat{n}_d \rangle_0 = 2\delta(0)/\pi$ yields

$$\lim_{\phi \to 0} Q_{\mathrm{loc}}(\phi; T = 0) = -\frac{2 \operatorname{sgn} \phi}{\pi} \operatorname{arccot}(\pi \bar{\rho}_0 W_d). \tag{72}$$

The latter relation explains the equality of the exponents β entering Eqs. (52) and (71). It should also be noted that Eqs. (65), (66), and (72) together imply that

$$\lim_{\phi \to 0} Q_{\mathrm{loc}}^2(\phi; T = 0) = \lim_{T \to 0} T\chi_{c,\mathrm{imp}}(T). \tag{73}$$

At the critical point, the response to a small-but-finite potential ϕ obeys another power law,

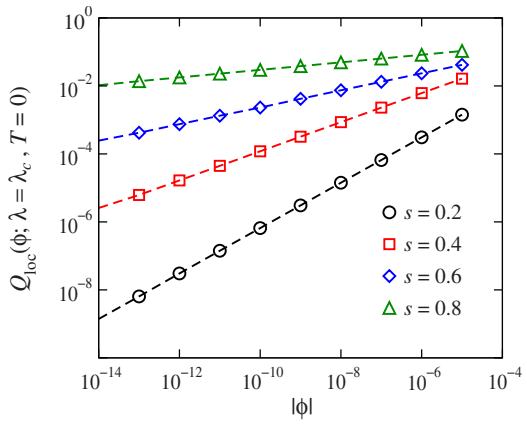

FIG. 13. (Color online) Impurity charge $Q_{\rm loc}(\phi;\lambda=\lambda_c,T=0)$ vs local electric potential $|\phi|$ for four different values of the bath exponent s. All other parameters are as in Fig. 5. The dashed lines represent fits to the form of Eq. (74).

$$Q_{\rm loc}(\phi;\lambda=\lambda_c,T=0)\propto|\phi|^{1/\delta}. \tag{74}$$

This behavior is exemplified in Fig. 13 for four different values of s.

Figure 14 shows a logarithmic plot of the static local charge susceptibility $\chi_{c,\rm loc}(T;\omega=0)$ vs temperature T for bath exponent $s=0.4$ and a number of e-b couplings straddling λ_c. In the quantum-critical regime, the susceptibility has the anomalous temperature dependence

$$\chi_{c,\rm loc}(T;\omega=0)\propto T^{-x}\quad \text{for } T_*\ll T\ll T_{\rm K}, \tag{75}$$

characterized by a critical exponent x. For $T\ll T_*(\lambda)$, the temperature variation approaches that of one or other of the stable fixed points. In the Kondo phase, the susceptibility is essentially temperature independent, signaling complete quenching of the impurity, and the zero-temperature value diverges on approach to the critical coupling as

$$\chi_{c,\rm loc}(\lambda;\omega=T=0)\propto(\lambda_c-\lambda)^{-\gamma}\quad \text{for } \lambda\to\lambda_c^-. \tag{76}$$

In the localized phase, by contrast,

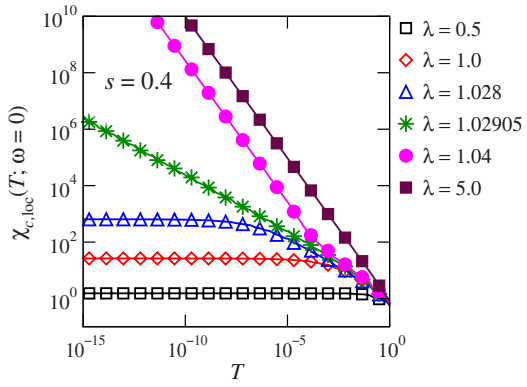

FIG. 14. (Color online) Static local charge susceptibility $\chi_{c,\rm loc}(T;\omega=0)$ vs temperature T for $s=0.4$, $U=-2\epsilon_d=0.1$, $\Gamma=1.0$ (see footnote 56), $\Lambda=9$, $N_s=500$, $N_b=8$, and for different values of the e-b coupling λ straddling the critical value $\lambda_c\simeq 1.029\,05$.

TABLE III. Static critical exponents β, $1/\delta$, x, and γ defined in Eqs. (71) and (74)–(76), respectively, for four different values of the bosonic bath exponent s. Parentheses surround the estimated nonsystematic error in the last digit.

s	β	$1/\delta$	x	γ
0.2	2.0005(3)	0.6673(1)	0.1997(2)	0.997(4)
0.4	0.7568(2)	0.4283(2)	0.4002(4)	1.0117(6)
0.6	0.3923(1)	0.2501(7)	0.600(2)	1.1805(5)
0.8	0.2130(1)	0.1111(1)	0.800(2)	1.703(3)

$$\chi_{c,\rm loc}(T,\lambda;\omega=0)=\lim_{\phi\to0}\frac{Q^2_{\rm loc}(\lambda,\phi;T=0)}{T}$$

$$\text{for } \lambda>\lambda_c \text{ and } T\ll T_*, \tag{77}$$

indicative of a residual impurity degree of freedom. Precisely at the critical e-b coupling, Eq. (75) is obeyed all the way down to $T=0$.

Table III lists the numerical values of the critical exponents β, $1/\delta$, x, and γ, for four different sub-Ohmic bath exponents s. For each s, these critical exponents are identical within estimated error to those of the spin-boson and Ising BFK models. In all cases, we find that $x=s$ to within our estimated nonsystematic numerical error. We also note that for $s\leqslant\frac{1}{2}$, the value of γ lies close to its mean-field value of 1. It is conceivable that the deviations of γ from 1 are artifacts of the NRG discretization and truncation approximations.

The exponents in Table III obey the hyperscaling relations

$$\delta=\frac{1+x}{1-x},\quad 2\beta=\nu(1-x),\quad \gamma=\nu x, \tag{78}$$

which are consistent with the ansatz

$$F=Tf\left(\frac{|\lambda-\lambda_c|}{T^{1/\nu}},\frac{|\phi|}{T^{(1+x)/2}}\right) \tag{79}$$

for the nonanalytic part of the free energy. Such hyperscaling suggests that the quantum critical point is an interacting one.[4]

2. Dynamical local charge susceptibility

The dynamical local charge susceptibility is

$$\chi_{c,\rm loc}(\omega,T)=i\int_0^\infty dt\,e^{-i\omega t}\langle\langle[\hat n_d(t)-1,\hat n_d(0)-1]\rangle\rangle. \tag{80}$$

Its imaginary part $\chi''_{c,\rm loc}$ can be calculated within the NRG as

$$\chi''_{c,\rm loc}(\omega,T)=\frac{\pi}{Z(T)}\sum_{m,m'}|\langle m'|\hat n_d-1|m\rangle|^2(e^{-E_{m'}/T}-e^{-E_m/T})$$
$$\times\delta(\omega-E_{m'}+E_m). \tag{81}$$

Here, $|m\rangle$ is a many-body eigenstate with energy E_m, and $Z(T)=\Sigma_m e^{-E_m/T}$ is the partition function. Equation (81) pro-

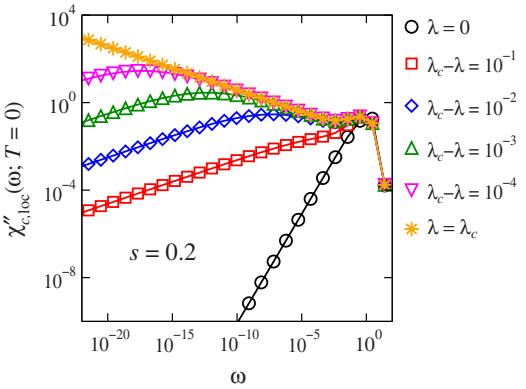

FIG. 15. (Color online) Imaginary part of the dynamical local charge susceptibility $\chi''_{c,\mathrm{loc}}(\omega;T=0)$ vs frequency ω for $s=0.2$, $U=-2\epsilon_d=0.1$, $\Gamma=0.5$ (see footnote 56), $\Lambda=9$, $N_s=500$, $N_b=8$, and different *e-b* couplings $\lambda<\lambda_c$ on the Kondo side of the critical point, which is located at $\lambda_c\simeq 0.530\,08$. As $\lambda\to\lambda_c^-$, $\chi''_{c,\mathrm{loc}}(\omega;T=0)$ follows the quantum critical form [Eq. (83)] for $T_*\ll\omega\ll T_\mathrm{K}$, where T_K is the Kondo scale of the pure-fermionic ($\lambda=0$) problem.

duces a discrete set of delta-function peaks that must be broadened to recover a continuous spectrum. Following standard procedure,[59] we employ Gaussian broadening of delta functions on a logarithmic scale,

$$\delta(|\omega|-|\Delta E|)\to\frac{e^{-b^2/4}}{\sqrt{\pi}b|\Delta E|}\exp\left[-\frac{(\ln|\omega|-\ln|\Delta E|)^2}{b^2}\right], \tag{82}$$

with the choice of the broadening width $b=0.5\ln\Lambda$.

(a) *Zero temperature.* Figure 15 plots $\chi''_{c,\mathrm{loc}}(\omega;T=0)$ vs ω for bath exponent $s=0.2$ and a series of *e-b* couplings $\lambda<\lambda_c$. Whereas $\chi''_{c,\mathrm{loc}}(\omega;\lambda=0,T=0)\propto\omega$ for $|\omega|\ll T_\mathrm{K}$ (the usual Kondo result), we find that $\chi''_{c,\mathrm{loc}}(\omega;0<\lambda<\lambda_c,T=0)\propto|\omega|^s\,\mathrm{sgn}(\omega)$ as $\omega\to 0$, corresponding to a long-time relaxation behavior $\chi_{c,\mathrm{loc}}(t)\propto t^{-(1+s)}$. Precisely at the critical *e-b* coupling,

$$\chi''_{c,\mathrm{loc}}(\omega;\lambda=\lambda_c,T=0)\propto|\omega|^{-y}\,\mathrm{sgn}(\omega)\quad\text{for }\omega\ll T_\mathrm{K}. \tag{83}$$

Figure 16 shows $\chi''_{c,\mathrm{loc}}(\omega;\lambda=\lambda_c,T=0)$ vs ω and $\chi_{c,\mathrm{loc}}(T;\lambda=\lambda_c,\omega=0)$ vs T for representative bosonic bath exponents $s=0.2$ and $s=0.8$. These and all other data that we have obtained are consistent with the relation

$$x=y=s\quad\text{for }0<s<1. \tag{84}$$

For small deviations from the critical coupling, $\chi''_{c,\mathrm{loc}}(\omega;T=0)$ exhibits the critical behavior of Eq. (83) over the range $T_*\ll|\omega|\ll T_\mathrm{K}$, where T_* is identical (up to a constant multiplicative factor) to the crossover scale defined in Sec. IV C that vanishes at the quantum critical point according to Eq. (58).

(b) *Finite temperatures.* Equation (84) is consistent with the presence of ω/T scaling in the dynamical local charge susceptibility at the quantum critical point, viz,

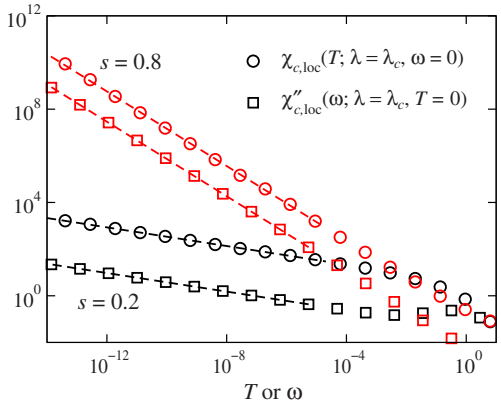

FIG. 16. (Color online) Critical static and dynamical response: $\chi_{c,\mathrm{loc}}(T;\lambda=\lambda_c,\omega=0)$ vs T (circles) and $\chi''_{c,\mathrm{loc}}(\omega;\lambda=\lambda_c,T=0)$ vs ω (squares) for two representative bath exponents $s=0.2$ and $s=0.8$. All other parameters are as in Fig. 5. The equality of the slopes of the static and dynamical charge susceptibilities for a given bath exponent s indicates that the corresponding critical exponents satisfy $x=y$.

$$\chi''_{c,\mathrm{loc}}(\omega,T;\lambda=\lambda_c)=T^{-s}\Psi_s(\omega/T). \tag{85}$$

Figure 17 shows the collapse of data for $\chi''_{c,\mathrm{loc}}(\omega,T;\lambda=\lambda_c)$ onto a single function of ω/T within the critical regime. The Kondo temperature T_K of the Anderson model obtained by setting $\lambda=0$ serves as a nonuniversal high-frequency cutoff on the critical behavior; the curves have a common form for $\omega/T\ll T_\mathrm{K}/T$. It should be noted that the NRG method is unreliable[52,60] for $|\omega|\lesssim T$, preventing demonstration of complete ω/T scaling.

Both the hyperscaling of the static critical exponents and what seems to be ω/T scaling of the dynamical susceptibility are consistent with the QPT between the Kondo and localized phases taking place at an interacting critical point below its upper critical dimension.

F. Impurity spectral function

We now turn to discussion of the impurity spectral function $A_\sigma(\omega,T)=-\pi^{-1}\,\mathrm{Im}\,G_{d\sigma}(\omega,T)$, where the retarded impurity Green's function is

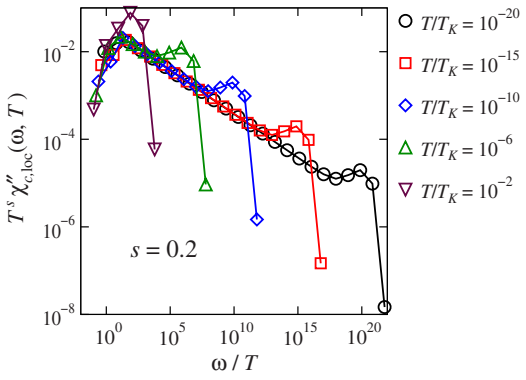

FIG. 17. (Color online) Scaling with ω/T of the imaginary part of the dynamical local charge susceptibility $\chi''_{c,\mathrm{loc}}(\omega,T)$ at the critical *e-b* coupling $\lambda_c\simeq 0.530\,08$ for $s=0.2$, $U=-2\epsilon_d=0.1$, $\Gamma=0.5$ (see footnote 56), $\Lambda=9$, $N_s=500$, $N_b=8$, and different temperatures $T\ll T_K=0.425$.

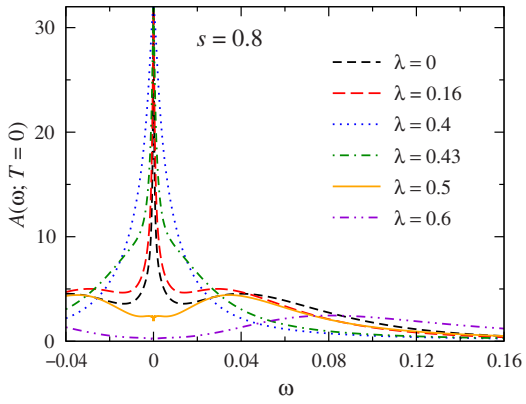

FIG. 18. (Color online) Impurity spectral function $A(\omega;T=0)$ vs frequency ω for $s=0.8$, $U=-2\epsilon_d=0.1$, $\Gamma=0.01$, $\Lambda=3$, $N_s=1200$, $N_b=8$, and different values of the e-b coupling λ. For these parameters, $U_{\rm eff}$ defined in Eq. (33) changes sign at $\lambda_{c0}\simeq 0.369$ and the critical coupling is $\lambda_c\simeq 0.474$.

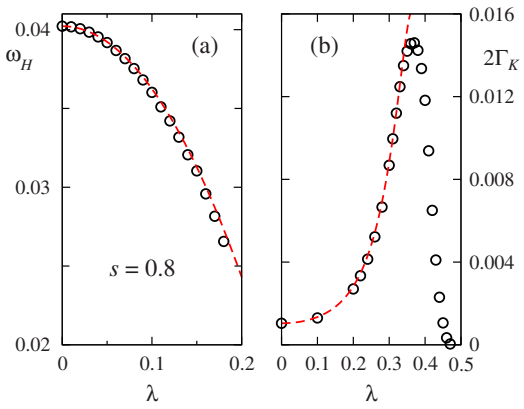

FIG. 19. (Color online) Variation with e-b coupling λ of two characteristic energy scales extracted from the zero-temperature impurity spectral function. All parameters except λ are the same as in Fig. 18. (a) Location ω_H of the upper Hubbard peak. The dashed line shows $\omega_H=0.4U-\lambda^2/(\pi s)$. (b) Kondo resonance width (full width at half height) $2\Gamma_{\rm K}$. The dashed line, representing the prediction of Eq. (88) with $C_{\rm K}=0.82$ and with $\tilde{U}^{\rm NRG}$ in Eq. (48) evaluated at $E=U/2=|\epsilon_d|$, fits the data over almost the entire range $0\leqslant\lambda<\lambda_{c0}\simeq 0.369$.

$$G_{d\sigma}(\omega,T)=-i\int_0^\infty dt\, e^{i\omega t}\langle\langle[d_\sigma(t),d_\sigma^\dagger(0)]_+\rangle\rangle. \tag{86}$$

The spectral function can be calculated within the NRG using the formulation

$$A_\sigma(\omega,T)=\frac{1}{Z(T)}\sum_{m,m'}|\langle m'|d_\sigma^\dagger|m\rangle|^2(e^{-E_{m'}/T}+e^{-E_m/T})\times\delta(\omega-E_{m'}+E_m), \tag{87}$$

where the notation is the same as in Eq. (81). To recover a continuous spectrum, we have again applied Eq. (82) to the delta-function output of Eq. (87), choosing the broadening factor $b=0.55\ln\Lambda$ that best satisfies the Fermi-liquid result $A_\sigma(\omega=0,T=0)=1/\pi\Gamma$ for the Anderson model. In order to achieve satisfactory results, we find it necessary to work with a smaller discretization parameter ($\Lambda=3$ instead of the value $\Lambda=9$ employed for all the quantities reported above) and to retain more states ($N_s=1200$ rather than the 500 that typically suffices). Since the spectral functions shown below are all spin independent, we henceforth drop the index σ on A_σ. For the particle-hole-symmetric model considered in this section, the spectral function is symmetric about $\omega=0$.

Figure 18 plots $A_\sigma(\omega;T=0)$ vs ω for $s=0.8$ and a series of λ values. For $\lambda=0$, we recover the spectral function of the Anderson model, featuring a narrow Kondo resonance centered at zero frequency and broad Hubbard satellite bands centered around $\omega=\pm\frac{1}{2}U$. Increasing the e-b coupling from zero has two initial effects—a displacement of the Hubbard bands to smaller frequencies, and a broadening of the low-energy Kondo resonance—that can both be attributed to the boson-induced renormalization of the Coulomb interaction described in Eq. (46).

We expect the Hubbard peak locations to obey $\omega_H\simeq\pm\frac{1}{2}U_{\rm eff}$ for $0\leqslant\lambda\ll\lambda_{c0}$. However, the peak locations plotted in Fig. 19(a) are better fitted by $|\omega_H|=0.4U-\lambda^2/(\pi s)$, which (given the discretization and truncation effects discussed in Sec. III A) appears to represent a stronger bosonic renormalization than that predicted by $|\omega_H|=\frac{1}{2}U_{\rm eff}$. We believe that this discrepancy arises primarily from the rapid broadening of the Kondo resonance with increasing λ, which shifts the local maximum of the combined spectral function (the sum of the Kondo resonance plus Hubbard satellite bands) to a frequency smaller in magnitude than the central frequency of the Hubbard peak by itself.

The width $2\Gamma_{\rm K}$ of the Kondo resonance, plotted in Fig. 19(b), proves to be equal (up to a multiplicative constant) to the crossover scale T_* defined in Sec. IV C. For $\lambda\lesssim\lambda_{c0}$, the variation in both scales is well described by the replacement of U in the expression[20] for the Kondo temperature of the symmetric Anderson model by $\tilde{U}^{\rm NRG}(U/2)$ [given by Eq. (48)], the effective Coulomb interaction on entry to the local-moment regime. The dashed line in Fig. 19(b) shows that the resulting formula,

$$\Gamma_{\rm K}=C_{\rm K}\sqrt{\frac{8\tilde{U}^{\rm NRG}\Gamma}{\pi A_\Lambda}}\exp\left(-\frac{\pi A_\Lambda\tilde{U}^{\rm NRG}}{8\Gamma}\right), \tag{88}$$

where A_Λ is defined in Eq. (31), provides an excellent description of $\Gamma_{\rm K}$ over almost the entire range $0\leqslant\lambda<\lambda_{c0}\simeq 0.369$. This echoes the finding in the Anderson-Holstein model that a weak e-b coupling serves primarily to reduce the impurity on-site repulsion, leading to an increase in the Kondo scale.[8]

Once the e-b coupling exceeds λ_{c0}, further increase in λ leads to suppression of the Hubbard peaks (e.g., see the curves for $\lambda=0.4$ and $\lambda=0.43$ in Fig. 18) and to a rapid narrowing of the Kondo resonance [see Fig. 19(b)]. In the Anderson-Holstein model, the Kondo scale remains nonzero—although exponentially reduced—for arbitrarily large e-b couplings.[8] In the charge-coupled BFA model, by contrast, the Kondo peak collapses and $\Gamma_{\rm K}$ extrapolates to zero as λ approaches its critical value λ_c. As shown in

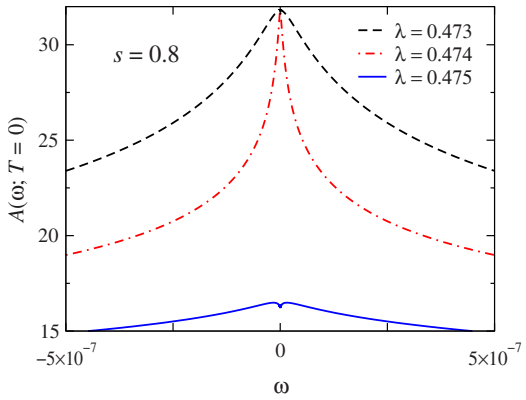

FIG. 20. (Color online) Detail of the impurity spectral function $A(\omega;T=0)$ around frequency $\omega = 0$ for $s=0.8$, $U=-2\epsilon_d=0.1$, $\Gamma=0.01$, $\Lambda=3$, $N_s=1600$, $N_b=8$, and different *e-b* couplings λ straddling the critical value $\lambda_c \simeq 0.474\,58$. For $\lambda \leqslant \lambda_c$, $A(\omega;T=0)$ is pinned to the value predicted by Fermi-liquid theory. For $\lambda > \lambda_c$, the Kondo resonance disappears, leaving a pair of low-energy peaks centered at $|\omega|$ of order the crossover temperature T_* ($\simeq 1.4\times 10^{-8}$ for $\lambda=0.475$).

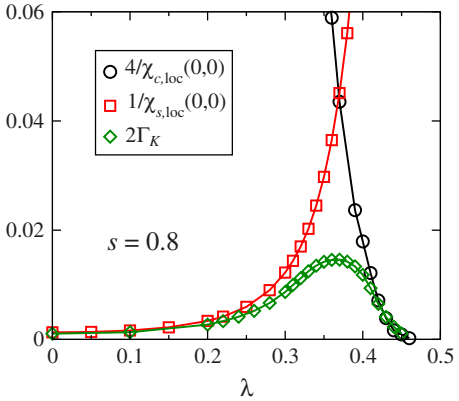

FIG. 21. (Color online) Variation with *e-b* coupling $\lambda < \lambda_c$ of the Kondo resonance width $2\Gamma_K$, the inverse static local spin susceptibility $1/\chi_{s,\mathrm{loc}}(\omega=0,T=0)$, and the inverse static local charge susceptibility $4/\chi_{c,\mathrm{loc}}(\omega=0,T=0)$. The results shown are for $s=0.8$, $U=-2\epsilon_d=0.1$, $\Gamma=0.01$, $\Lambda=3$, $N_s=1200$, and $N_b=8$. For the calculation of the static local spin susceptibility via Eq. (89), the total spin S is not a good quantum number, so N_s specifies the number of (S_z,Q) states retained after each iteration.

Fig. 20, the central peak remains pinned to the Fermi-liquid result $A(\omega=0,T=0)=1/\pi\Gamma$ even as the peak width vanishes for $\lambda \to \lambda_c^-$.

In the localized phase ($\lambda > \lambda_c$), there is no vestige of the Kondo resonance, but high-energy Hubbard-like peaks reappear; see the curves for $\lambda=0.5$ and $\lambda=0.6$ in Fig. 18. In addition, there is a pair of low-energy peaks centered at $\omega \simeq \pm T_*$, as shown in Fig. 20.

G. Spin-Kondo to charge-Kondo crossover

Based on the analysis of the zero-hybridization limit presented in Sec. III A, one expects spin fluctuations to dominate the impurity behavior in the region $\lambda \ll \lambda_{c0}$, but charge fluctuations to be dominant for $\lambda_{c0} \ll \lambda < \lambda_c$. This picture is supported by the behaviors of the thermodynamic susceptibilities discussed in Sec. IV D. The evolution from a spin-Kondo effect to a charge-Kondo effect can also be probed by comparing the static local charge susceptibility [Eq. (70)] with its spin counterpart

$$\chi_{s,\mathrm{loc}}(T;\omega=0) = -\lim_{h\to 0} \frac{\langle\langle \hat{n}_{d\uparrow} - \hat{n}_{d\downarrow}\rangle\rangle}{2h}, \tag{89}$$

where h is a local magnetic field that enters an additional Hamiltonian term

$$\hat{H}_{s,\mathrm{loc}} = \frac{h}{2}(\hat{n}_{d\uparrow} - \hat{n}_{d\downarrow}). \tag{90}$$

In particular, characteristic energy scales for the spin and charge Kondo effects are expected to be $1/\chi_{s,\mathrm{loc}}(\omega=0,T=0)$ and $4/\chi_{c,\mathrm{loc}}(\omega=0,T=0)$, respectively [where the factor of 4 accounts for the difference in conventions that ϕ couples to $\hat{n}_d-1$, whereas h couples to $(\hat{n}_{d\uparrow}-\hat{n}_{d\downarrow})/2$]. Figure 21 plots the λ dependence of these quantities for the parameter set illustrated in Figs. 18 and 19. The Kondo resonance width $2\Gamma_K$ crosses over from paralleling $1/\chi_{s,\mathrm{loc}}(0,0)$ for small λ to loosely tracking[61] $4/\chi_{c,\mathrm{loc}}(0,0)$ as λ approaches λ_c. In the intermediate region near $\lambda=\lambda_{c0}$, $2\Gamma_K$ is much smaller than either inverse static susceptibility, indicating that the Kondo effect has mixed spin and charge character.

Figure 22 presents a λ-Γ phase diagram for $s=0.8$ and fixed $U=-2\epsilon_d$, showing data points along the phase boundary $\lambda=\lambda_c(\Gamma)$ and along the crossover boundary $\lambda=\lambda_X(\Gamma)$, defined as the *e-b* coupling at which the Kondo resonance width $2\Gamma_K$ is maximal for the given Γ. The fact that the latter line rises almost vertically from $\lambda=\lambda_{c0}$ at $\Gamma=0$ provides further confirmation of the picture of a crossover from a spin-Kondo effect to a charge-Kondo effect resulting from the change in the sign of U_{eff} and establishes the validity of the schematic phase diagram (Fig. 3) presented in the introduction to this section.

V. RESULTS: SYMMETRIC MODEL WITH OHMIC DISSIPATION

This section presents results for Hamiltonian (1) with $U=-2\epsilon_d>0$ and an Ohmic bath (i.e., $s=1$). We first discuss the

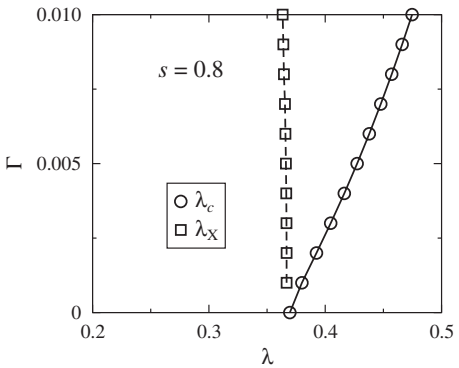

FIG. 22. Phase boundary $\lambda_c(\Gamma)$ and crossover boundary $\lambda_X(\Gamma)$ (defined in the text) for $s=0.8$, $U=-2\epsilon_d=0.1$, $\Lambda = 3$, $N_s=1200$, and $N_b=8$. The data are consistent with the schematic phase diagram shown in Fig. 3.

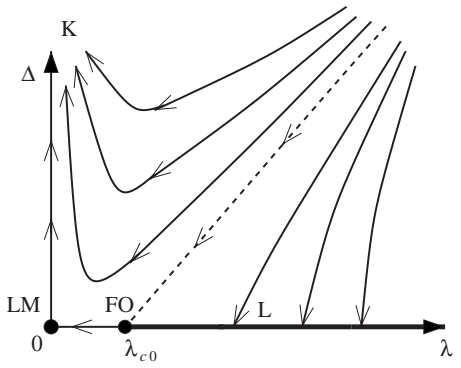

FIG. 23. Schematic renormalization-group flows on the λ-Δ plane for the symmetric model with bath exponent $s=1$. Trajectories represent the flow of the couplings λ entering Eq. (15) and Δ defined in Eq. (50) under decrease in the high-energy cutoffs on the conduction band and the bosonic bath. A separatrix (dashed line) forms the boundary between the basins of attraction of the Kondo fixed point (K) and a line of localized fixed points (L). Flow along the separatrix is toward the free-orbital fixed point (FO) located at $\lambda=\lambda_{c0}$. For $\Delta=0$ only, there is flow away from FO toward the local-moment fixed point (LM) at $\lambda=0$.

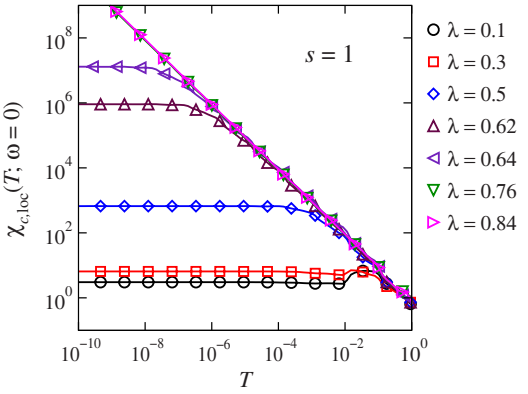

FIG. 24. (Color online) Static local charge susceptibility $\chi_{c,\mathrm{loc}}(T;\omega=0)$ vs temperature T for $s=1$, $U=-2\epsilon_d=0.1$, $\Gamma=0.01$, $\Lambda=9$, $N_s=800$, $N_b=12$, and different e-b couplings λ. On the Kondo side of the QPT ($\lambda<\lambda_c\simeq 0.726$), there is a clear crossover from quantum-critical to screened behavior around the renormalized Kondo temperature $T_*=4/\chi_{c,\mathrm{loc}}(\omega=T=0)$. No such crossover is evident on the localized side ($\lambda>\lambda_c$).

behavior of the static local charge susceptibility. We show that, in contrast with the sub-Ohmic case $0<s<1$, the crossover scale vanishes in exponential (rather than power-law) fashion as the e-b coupling approaches its critical value from below, and there is no small energy scale observed on the localized side of the transition. Therefore, the QPT for the Ohmic case is of Kosterlitz-Thouless type. At the end of the section, we study the effects of the e-b coupling on the impurity spectral function.

A. Fixed points and thermodynamic susceptibilities

Figure 23 plots the schematic renormalization-group flows for a symmetric impurity coupled to an Ohmic bath. The flows within the Kondo basin of attraction are qualitatively very similar to those for the sub-Ohmic case depicted in Fig. 4. In the localized regime, however, the e-b coupling flows not to $\lambda=\infty$ but rather to a finite limiting value that varies continuously with the bare values of λ and Γ. What is shown as a line of fixed points in Fig. 23 is really a plane of fixed points described by $\hat{H}_{\mathrm{LC}}$ [Eq. (49)] with effective couplings $\lambda>\lambda_{c0}$, $W_p=0$, and $0\leqslant W_d<\infty$. Another important departure from the sub-Ohmic case is that for $s=1$ there is no longer a distinct critical point reached by flow along the separatrix from the free-orbital fixed point; rather these two fixed points merge as $s\to 1^-$, leaving a critical endpoint at $\lambda=\lambda_{c0}$, $\Delta=0$. Strictly, this is a line of critical endpoints described by $\hat{H}_{\mathrm{LC}}$ [Eq. (49)] with effective couplings $\lambda=\lambda_{c0}$, $W_p=0$, and $0\leqslant W_d<\infty$. For a fixed bare value of Γ, the endpoint value of W_d is just the limit of the localized fixed-point value of W_d as the bare coupling λ approaches the phase boundary $\lambda_c(\Gamma)$.

The behaviors of the static impurity spin and charge susceptibilities are qualitatively very similar to those for a sub-Ohmic bath, as discussed in Sec. IV D. The only significant difference is that for $s=1$, $\lim_{T\to 0} T\chi_{c,\mathrm{imp}}(T)$ undergoes a discontinuous jump from its value of 0 for $\lambda\leqslant\lambda_c$ to a nonzero value for $\lambda=\lambda_c^+$. This jump can be understood through Eqs. (65) and (66) as a consequence of the fact that W_d does not diverge on approach to the critical coupling.

B. Static local charge susceptibility and crossover scale

Figure 24 is a logarithmic plot of the static local charge susceptibility $\chi_{c,\mathrm{loc}}(T;\omega=0)$ vs temperature T for different e-b couplings λ. On the Kondo side of the phase boundary, $\chi_{c,\mathrm{loc}}(T;\omega=0)$ is proportional to $1/T$ at high temperatures but levels off for $T\lesssim T_*$. We find it convenient to *define*

$$T_* = 4/\chi_{c,\mathrm{loc}}(\omega=T=0) \quad \text{for } \lambda\to\lambda_c^-, \tag{91}$$

thereby removing the ambiguity in the definition of the crossover iteration N_* (see Sec. IV C) on the Kondo side of the $s=1$ quantum phase transition.

For $\lambda\to\lambda_c^-$, the crossover scale vanishes according to (see Fig. 25)

$$T_* \propto \exp\left[-\frac{C_*}{\sqrt{1-(\lambda/\lambda_c)^2}}\right]. \tag{92}$$

In the localized phase, $\chi_{c,\mathrm{loc}}(T;\omega=0)$ satisfies Eq. (77) over the entire temperature range $T\ll U$. Since the critical and localized fixed points share the same temperature variation, no crossover scale can be identified on the localized side of the phase boundary. Moreover, the order parameter $\lim_{\phi\to 0} Q_{\mathrm{loc}}(\phi;T=0)$ does not vanish continuously as $\lambda\to\lambda_c^+$ but rather undergoes a discontinuous jump at the transition, as shown in Fig. 25. The magnitude of this jump is nonuniversal, being related via Eq. (72) to the value of W_d at the critical endpoint.

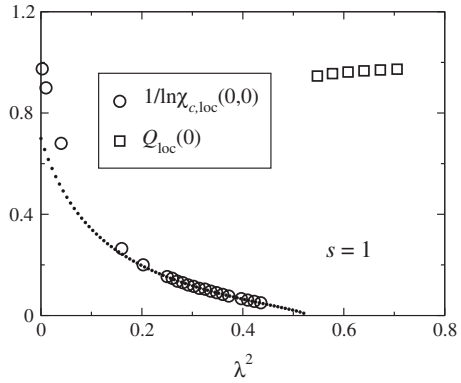

FIG. 25. Variation with e-b coupling λ of the local charge susceptibility $\chi_{c,\mathrm{loc}}(\omega=T=0)$ in the Kondo phase $\lambda<\lambda_c\simeq 0.726$ and of the order parameter $\lim_{\phi\to 0} Q_{\mathrm{loc}}(\phi;T=0)$ in the localized phase $\lambda>\lambda_c$ for $s=1$, $U=-2\epsilon_d=0.1$, $\Gamma=0.01$, $\Lambda=9$, $N_s=800$, and $N_b=12$. The dotted line shows a fit of the susceptibility data using Eqs. (91) and (92).

The properties described above are analogous to those of the Kondo model [Eq. (39)] at the transition between the Kondo-screened phase (reached for $J_\perp\neq 0$ and $J_z>-|J_\perp|$) and the local-moment phase (reached for $J_z\leqslant -|J_\perp|$). Such behaviors are characteristic of a Kosterlitz-Thouless type of QPT.

C. Impurity spectral function

Figure 26 shows the impurity spectral function $A(\omega;T=0)$ for an Ohmic bath. The behavior in the Kondo phase is similar to that in the sub-Ohmic case discussed in Sec. IV F. As the e-b coupling λ increases from zero, the Hubbard satellite bands are initially displaced to smaller frequencies according to $\omega_H\simeq\pm\frac{1}{2}U_{\mathrm{eff}}$ [Fig. 27(a)], while the width $2\Gamma_{\mathrm{K}}$ of the Kondo resonance [Fig. 27(b)] first rises before falling sharply on approach to $\lambda=\lambda_c$. Just as for $0<s<1$, the variation in Γ_{K} for $\lambda\lesssim\lambda_{c0}$ is well described by Eq. (88) with $\tilde{U}^{\mathrm{NRG}}$ [Eq. (48)] evaluated at $E=U/2$. Throughout the Kondo phase, $A(\omega=T=0)$ remains pinned at its Fermi-liquid value $1/\pi\Gamma$.

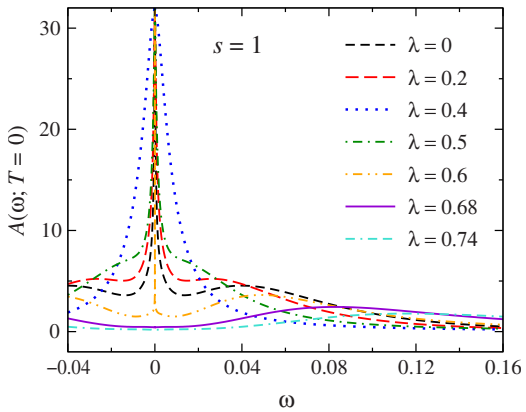

FIG. 26. (Color online) Impurity spectral function $A(\omega;T=0)$ vs ω for $s=1$, $U=-2\epsilon_d=0.1$, $\Gamma=0.01$, $\Lambda=3$, $N_s=1200$, $N_b=12$, and different values of the e-b coupling λ. For these parameters, U_{eff} [Eq. (33)] changes sign at $\lambda_{c0}\simeq 0.413$ and the critical coupling is $\lambda_c\simeq 0.669$.

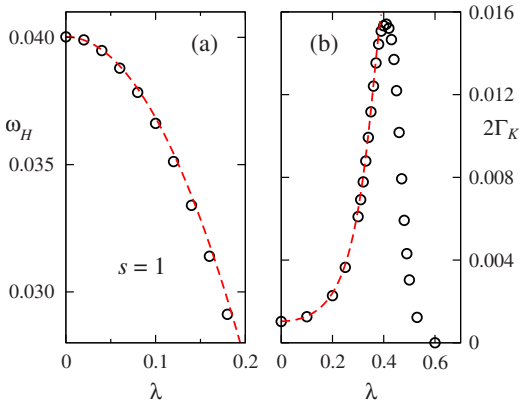

FIG. 27. (Color online) Variation with e-b coupling λ of two characteristic energy scales extracted from the zero-temperature impurity spectral function. All parameters except λ are the same as in Fig. 26. (a) Location ω_H of the upper Hubbard peak. The dashed line shows $\omega_H(\lambda)=0.4U-\lambda^2/\pi$. (b) Kondo resonance width (full width at half height) $2\Gamma_{\mathrm{K}}$. The dashed line, representing the prediction of Eq. (88) with $C_{\mathrm{K}}=0.82$ and with $\tilde{U}^{\mathrm{NRG}}$ in Eq. (48) evaluated at $E=U/2=|\epsilon_d|$, fits the data over almost the entire range $0\leqslant\lambda<\lambda_{c0}\simeq 0.413$.

For $\lambda\geqslant\lambda_c$, however, the behavior of the spectral function is quite different for $s=1$ than for $0<s<1$. In the sub-Ohmic case, the Kondo-phase pinning extends to the quantum critical point, i.e., $\pi\Gamma A(\omega=T=0,\lambda=\lambda_c)=1$, while in the localized phase peaks appear at $\omega\simeq\pm T_*$. Figure 28 shows that the Ohmic spectral function instead satisfies $\pi\Gamma A(\omega=T=0,\lambda=\lambda_c)<1$ and exhibits no feature in the localized phase at energy scales much smaller than $\frac{1}{2}|U_{\mathrm{eff}}|$.

VI. RESULTS: ASYMMETRIC MODEL

Sections IV and V focused exclusively on results for a symmetric impurity satisfying $\epsilon_d=-U/2$ in Eq. (2) or,

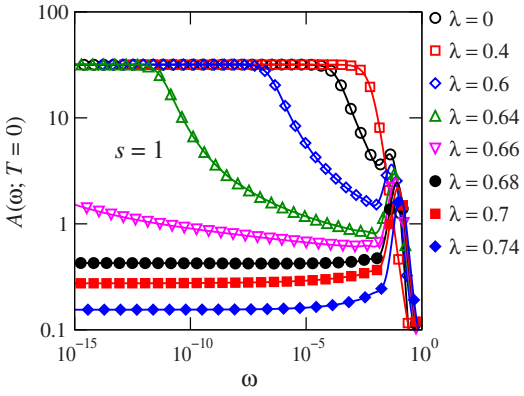

FIG. 28. (Color online) Impurity spectral function $A(\omega;T=0)$ vs frequency ω on a logarithmic scale for $s=1$, $U=-2\epsilon_d=0.1$, $\Gamma=0.01$, $\Lambda=3$, $N_s=1200$, $N_b=12$, and different e-b couplings λ. For $\lambda<\lambda_c\simeq 0.669$, the behavior is similar to that found for $0<s<1$. However, for $\lambda\geqslant\lambda_c$, the spectral function is essentially featureless below the energy scale $\frac{1}{2}|U_{\mathrm{eff}}|$ of the Hubbard peaks.

equivalently, $\delta_d=0$ in Eq. (9). We now turn to the general situation of an asymmetric impurity, starting with the sub-Ohmic case $0<s<1$.

For $\delta_d\neq 0$ and small, nonzero values of λ, one expects the fermionic sector of the charge-coupled BFA model to behave in essentially the same manner as in the asymmetric Anderson model (reviewed in Sec. III B), with the exception that the effective value of the Coulomb interaction U will be reduced by the coupling to the bosonic bath. At temperatures well below T_K, there will be no further renormalization of the electronic degrees of freedom, the system will exhibit quasiparticle excitations described by $\hat{H}_{SC}^{NRG}$ in Eq. (34), and the low-energy many-body states will share a nonvanishing expectation value $\langle \hat{n}_d-1\rangle[=Q_{loc}(T=0)]$. The bosons will couple to this impurity charge, yielding low-energy states described most naturally in terms of displaced-oscillator states [cf. Eq. (21)] annihilated by operators

$$\bar{a}_{\mathbf{q}} = a_{\mathbf{q}} + \frac{\lambda_{\mathbf{q}}}{\sqrt{N_q}\omega_{\mathbf{q}}}\langle \hat{n}_d - 1\rangle. \tag{93}$$

For $s<1$, the e-b coupling is relevant so λ will scale to strong coupling below a crossover temperature $T_L \ll T_K$.

For $\delta_d\neq 0$ and very large values of λ, one instead expects the bosons to localize the impurity at a high temperature scale T_L into a state with $\langle \hat{n}_d\rangle \simeq 0$ (for $\delta_d>0$) or $\langle \hat{n}_d\rangle \simeq 2$ (for $\delta_d<0$). For $T \lesssim T_L$, the impurity degrees of freedom will be frozen, the bosonic spectrum will rapidly approach strong coupling, and the conduction electrons will have an excitation spectrum corresponding to $\hat{H}_{FI}^{NRG}$ in Eq. (35) with a small value of $|V_0|$.

Given the equivalence of $\hat{H}_{SC}^{NRG}$ and $\hat{H}_{FI}^{NRG}$, it seems likely that the low-energy behavior of the asymmetric model will be the same in the small-λ and large-λ limits. This suggests that as the e-b coupling is increased from $\lambda=0^+$ to $\lambda\to\infty$, the many-body eigenstates evolve adiabatically without the occurrence of an intervening QPT.

For $s=1$, the e-b coupling is marginal, rather than relevant. One again expects a continuous evolution of the low-energy NRG spectrum with the bare value of λ. However, in this Ohmic case, the bosonic excitations should correspond to noninteracting displaced oscillators rather than the (truncated) strong-coupling spectrum found for $0<s<1$.

The preceding arguments are supported by our NRG results. Here, we illustrate just the case $s=0.4$. Figure 29 shows the variation with λ of the ground-state expectation value $\langle 1-\hat{n}_d\rangle_0$ for several values of δ_d. In the symmetric case (the $\delta_d=0$ curve in Fig. 29), the impurity charge vanishes throughout the Kondo phase, and grows in power-law fashion on entry to the localized phase. Away from particle-hole symmetry, by contrast, $\langle 1-\hat{n}_d\rangle_0$ increases smoothly from its Anderson-model value at $\lambda=0$ to approach 1 as $\lambda\to\infty$.

For all nonzero values of δ_d, Γ, and λ, the low-energy spectrum can be decomposed into the direct product of the fermionic spectrum corresponding to $\hat{H}_{SC}^{NRG}(V_1)$ [or $\hat{H}_{FI}^{NRG}(V_0)$] and the same localized-phase bosonic spectrum as

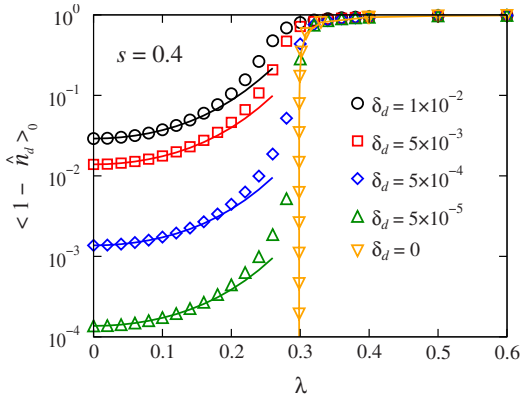

FIG. 29. (Color online) Variation in the magnitude $\langle 1-\hat{n}_d\rangle_0$ of the ground-state impurity charge with e-b coupling λ for $s=0.4$, $U=0.1$, $\Gamma=0.01$, $\Lambda=9$, $N_s=500$, and $N_b=8$. Symbols represent results for five values of the impurity asymmetry $\delta_d=\epsilon_d+U/2$. The solid lines corresponding to each case $\delta_d\neq 0$ represent the impurity charge calculated by solving the Anderson model [Eq. (11)] for the same δ_d value but using an effective Coulomb interaction $\tilde{U}^{NRG}(0.3U)$ [Eq. (48)]. The $\delta_d=0$ symbols show values of $\lim_{\phi\to 0^-} Q_{loc}(\lambda,\phi;T=0)$, connected by an interpolating line.

found for the symmetric model. The potential scattering V_1 (or V_0) is tied to $\langle \hat{n}_d-1\rangle_0$ by Eq. (37), just as in the Anderson model.

For small λ, the value of $\langle \hat{n}_d-1\rangle_0$ can be related to the corresponding quantity in the Anderson model by making use of the effective Coulomb interaction introduced in Sec. III A. In the asymmetric Anderson model, the ground-state charge becomes frozen once the system passes out of its mixed-valence regime, i.e., somewhat below a characteristic temperature T_f defined[20] for $\Gamma \ll -\epsilon_d \ll U$ as the solution of

$$T_f = |\epsilon_d| - \frac{\Gamma}{\pi}\ln\frac{U}{T_f}. \tag{94}$$

In the charge-coupled BFA model, U and ϵ_d in Eq. (94) should presumably be replaced by $\tilde{U}(T_f)$ and $\delta_d-\frac{1}{2}\tilde{U}(T_f)$, respectively. However, it suffices for our purposes to note that T_f can be expected to be of the same order as, but somewhat smaller than, $|\epsilon_d|$. It is then reasonable to hypothesize that $\langle n_d-1\rangle_0$ in the asymmetric charge-coupled BFA model should be close to the ground-state impurity charge of the Anderson model with the same Γ and δ_d but with U replaced by $\tilde{U}(E)$ [Eq. (47)] evaluated at $E\simeq T_f$. Our numerical results support this conjecture. For example, Fig. 29 shows that close to particle-hole symmetry ($\epsilon_d=-U/2$), the Anderson-model charge calculated for $\tilde{U}^{NRG}(E)$ [Eq. (48)] with $E=0.3U$ (solid lines) reproduces quite well the value of $\langle \hat{n}_d-1\rangle_0$ (symbols) over quite a broad range of e-b couplings $0\leqslant\lambda\lesssim\frac{2}{3}\lambda_c$, where $\lambda_c\simeq 0.298\,35$ is the critical coupling of the symmetric problem.

In the small-λ limit, one can also estimate the boson-localization temperature T_L by considering the evolution with decreasing T of the effective value of $\lambda\langle \hat{n}_d-1\rangle_0$. The impurity charge does not renormalize, while to lowest order

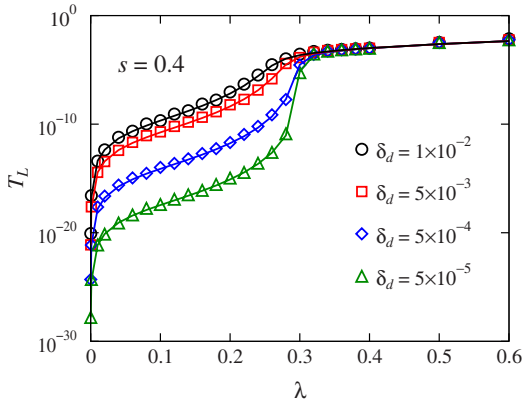

FIG. 30. (Color online) Variation in the bosonic localization temperature T_L with coupling λ for $s=0.4$, $U=0.1$, $\Gamma=0.01$, $\Lambda=9$, $N_s=500$, $N_b=8$, and various impurity asymmetries $\delta_d=\epsilon_d+U/2$. The solid lines were obtained by evaluating Eq. (95) with the $\langle 1-\hat{n}_d\rangle_0$ values shown in Fig. 29 and with $C_L=3$.

the effective e-b coupling obeys[45] Eq. (28). Defining T_L by the condition $\tilde{\lambda}(T_L)|\langle \hat{n}_d-1\rangle_0|=C_L$, we find

$$T_L \simeq |C_L^{-1}\lambda\langle \hat{n}_d-1\rangle_0|^{2/(1-s)}. \tag{95}$$

In Fig. 30, symbols represent T_L values extracted from the crossover of bosonic excitations in the NRG spectrum, while solid lines show the results of evaluating Eq. (95) using $C_L=3$ and the $\langle \hat{n}_d-1\rangle_0$ values shown in Fig. 29. The algebraic relation between the numerical values of T_L and $\langle 1-\hat{n}_d\rangle_0$ is well obeyed over a range of e-b couplings that extends beyond λ_c of the symmetric problem.

Figure 31 plots the static local charge susceptibility calculated for $s=0.4$ at the critical e-b coupling of the symmetric model. For $\delta_d\neq 0$, $\chi_{c,\mathrm{loc}}$ follows the quantum critical behavior $\chi_{c,\mathrm{loc}}(T;\omega=0)\propto T^{-x}$ from a high-temperature cutoff of order T_K down to a crossover temperature T_*, below which the susceptibility saturates. Based on Eq. (79) with the identification $\phi\equiv\delta_d$, one expects $T_*\propto|\delta_d|^{2/(1+x)}$ and, hence,

$$\chi_{c,\mathrm{loc}}(\phi;\lambda=\lambda_c,\omega=T=0)\propto|\delta_d|^{-2x/(1+x)}. \tag{96}$$

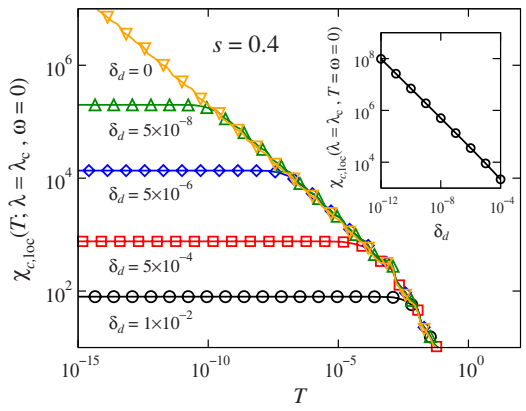

FIG. 31. (Color online) Static local charge susceptibility $\chi_{c,\mathrm{loc}}(T;\omega=0)$ vs temperature T for $s=0.4$, $U=0.1$, $\Gamma=0.01$, $\lambda\simeq 0.298\,35$, $\Lambda=9$, $N_s=500$, $N_b=8$, and various impurity asymmetries $\delta_d=\epsilon_d+U/2$. The e-b coupling equals the critical coupling λ_c of the symmetric case $\delta_d=0$. Inset: zero-temperature static local charge susceptibility $\chi_{c,\mathrm{loc}}(\omega=T=0)$ vs δ_d.

The log-log plot in the inset of Fig. 31 has a slope 0.57 that is fully consistent with Eq. (96).

The results of this work show that gaining direct access to the quantum critical point of the charge-coupled BFA model requires simultaneous fine tuning of two parameters: the e-b coupling λ as a function of the hybridization Γ and the on-site Coulomb repulsion U, and the particle-hole asymmetry (determined in our calculations solely by $\delta_d=\epsilon_d+U/2$, but in general also affected by the shape of the conduction-band density of states). While it may prove very challenging, or even impossible, to achieve this feat in any experimental realization of the model, it should be a more feasible task to carry out a rough tuning of parameters that places the system in the quantum critical regime over some window of elevated temperatures and/or frequencies.

VII. SUMMARY

We have conducted a detailed study of the charge-coupled Bose-Fermi Anderson model, in which a magnetic impurity both hybridizes with a structureless conduction band and is coupled, via its charge, to a dissipative environment represented by a bosonic bath having a spectral function that vanishes as ω^s for vanishing frequencies $\omega\to 0$. With increasing coupling between the impurity and the bath, we find a crossover from a conventional Kondo effect—involving conduction-band screening of the impurity spin degree of freedom—to a charge-Kondo regime in which the delocalized electrons quench impurity charge fluctuations.

Under conditions of strict particle-hole symmetry, further increase in the impurity-bath coupling gives rise for $0<s\leqslant 1$ to a quantum phase transition between the Kondo phase, in which the static charge and spin susceptibilities approach constant values at low temperatures, and a localized phase in which the static charge susceptibility exhibits a Curie-Weiss behavior indicative of an unquenched local charge degree of freedom. For sub-Ohmic bosonic bath spectra (described by an exponent s satisfying $0<s<1$), the continuous quantum phase transition is governed by an interacting critical point characterized by hyperscaling relations of critical exponents and ω/T scaling in the dynamical local charge susceptibility. Moreover, the continuous phase transition of the present model belongs to the same universality class as the transitions of the spin-boson and the Ising-anisotropic Bose-Fermi Kondo models. For an Ohmic ($s=1$) bosonic bath spectrum, the quantum phase transition is of Kosterlitz-Thouless type.

In the presence of particle-hole asymmetry, the quantum phase transition described in the previous paragraph is replaced by a smooth crossover, but for small-to-moderate asymmetries, signatures of the symmetric quantum critical point remain in the physical properties at elevated temperatures and/or frequencies. Investigation of the regime of strong particle-hole asymmetry, and of self-consistent versions of the charge-coupled Bose-Fermi Anderson model that arise with the extended dynamical mean-field theory of lattice fermions, will be pursued in future work.

ACKNOWLEDGMENTS

We thank Brian Lane for useful discussions. Much of the computational work was performed at the University of Florida High-Performance Computing Center. This work was supported in part by NSF Grants No. DMR-0710540 (M.C. and K.I.) and No. DMR-0706625 (M.T.G.).

*mxcheng@phys.ufl.edu

[1] A. C. Hewson, *The Kondo Problem to Heavy Fermions* (Cambridge University Press, Cambridge, UK, 1993).
[2] M. Vojta, Philos. Mag. **86**, 1807 (2006).
[3] S. L. Sondhi, S. M. Girvin, J. P. Carini, and D. Shahar, Rev. Mod. Phys. **69**, 315 (1997).
[4] S. Sachdev, *Quantum Phase Transitions* (Cambridge University Press, Cambridge, UK, 1999).
[5] D. Goldhaber-Gordon, H. Shtrikman, D. Mahalu, D. Abusch-Magder, U. Meirav, and M. A. Kastner, Nature (London) **391**, 156 (1998); W. G. van der Wiel, S. De Franceschi, T. Fujisawa, J. M. Elzerman, S. Tarucha, and L. P. Kouwenhoven, Science **289**, 2105 (2000); N. J. Craig, J. M. Taylor, E. A. Lester, C. M. Marcus, M. P. Hanson, and A. C. Gossard, *ibid.* **304**, 565 (2004); A. N. Pasupathy, R. C. Bialczak, J. Martinek, J. E. Grose, L. A. K. Donev, P. L. McEuen, and D. C. Ralph, *ibid.* **306**, 86 (2004); R. M. Potok, I. G. Rau, H. Shtrikman, Y. Oreg, and D. Goldhaber-Gordon, Nature (London) **446**, 167 (2007).
[6] H. Park, J. Park, A. K. L. Lim, E. H. Anderson, A. P. Alivisatos, and P. L. McEuen, Nature (London) **407**, 57 (2000); J. Park, A. N. Pasupathy, J. I. Goldsmith, C. Chang, Y. Yaish, J. R. Petta, M. Rinkoski, J. P. Sethna, H. D. Abruña, P. L. McEuen, and D. C. Ralph, *ibid.* **417**, 722 (2002); W. Liang, M. P. Shores, M. Bockrath, J. R. Long, and H. Park, *ibid.* **417**, 725 (2002); L. H. Yu and D. Natelson, Nano Lett. **4**, 79 (2004); L. H. Yu, Z. K. Keane, J. W. Ciszek, L. Cheng, M. P. Stewart, J. M. Tour, and D. Natelson, Phys. Rev. Lett. **93**, 266802 (2004); J. J. Parks, A. R. Champagne, G. R. Hutchison, S. Flores-Torres, H. D. Abruña, and D. C. Ralph, *ibid.* **99**, 026601 (2007).
[7] K. D. McCarthy, N. Prokof'ev, and M. T. Tuominen, Phys. Rev. B **67**, 245415 (2003); A. Mitra, I. Aleiner, and A. J. Millis, *ibid.* **69**, 245302 (2004).
[8] P. S. Cornaglia, H. Ness, and D. R. Grempel, Phys. Rev. Lett. **93**, 147201 (2004); P. S. Cornaglia, D. R. Grempel, and H. Ness, Phys. Rev. B **71**, 075320 (2005).
[9] J. Paaske and K. Flensberg, Phys. Rev. Lett. **94**, 176801 (2005); J. Mravlje, A. Ramšak, and T. Rejec, Phys. Rev. B **72**, 121403(R) (2005); K. A. Al-Hassanieh, C. A. Büsser, G. B. Martins, and E. Dagotto, Phys. Rev. Lett. **95**, 256807 (2005); J. Koch, M. E. Raikh, and F. von Oppen, *ibid.* **96**, 056803 (2006); J. Mravlje, A. Ramšak, and T. Rejec, Phys. Rev. B **74**, 205320 (2006); C. A. Balseiro, P. S. Cornaglia, and D. R. Grempel, *ibid.* **74**, 235409 (2006).
[10] R. Žitko and J. Bonča, Phys. Rev. B **74**, 224411 (2006).
[11] M. D. Nuñez Regueiro, P. S. Cornaglia, G. Usaj, and C. A. Balseiro, Phys. Rev. B **76**, 075425 (2007); M.-J. Hwang, M.-S. Choi, and R. López, *ibid.* **76**, 165312 (2007); P. S. Cornaglia, G. Usaj, and C. A. Balseiro, *ibid.* **76**, 241403(R) (2007); J. Mravlje, A. Ramšak, and R. Žitko, Physica B **403**, 1484 (2008); J. Mravlje and A. Ramšak, Phys. Rev. B **78**, 235416 (2008).
[12] L. G. G. V. Dias da Silva and E. Dagotto, Phys. Rev. B **79**, 155302 (2009).
[13] P. W. Anderson, Phys. Rev. **124**, 41 (1961).
[14] H. Kaga, I. Sato, and M. Kobayashi, Prog. Theor. Phys. **64**, 1918 (1980); K. Schönhammer and O. Gunnarsson, Phys. Rev. B **30**, 3141 (1984); B. Alascio, C. Balseiro, G. Ortíz, M. Kiwi, and M. Lagos, *ibid.* **38**, 4698 (1988); T. Östreich, *ibid.* **43**, 6068 (1991).
[15] A. C. Hewson and D. Meyer, J. Phys.: Condens. Matter **14**, 427 (2002); G. S. Jeon, T.-H. Park, and H.-Y. Choi, Phys. Rev. B **68**, 045106 (2003).
[16] H. C. Lee and H.-Y. Choi, Phys. Rev. B **69**, 075109 (2004); **70**, 085114 (2004).
[17] E. Šimánek, Solid State Commun. **32**, 731 (1979); C. S. Ting, D. N. Talwar, and K. L. Ngai, Phys. Rev. Lett. **45**, 1213 (1980).
[18] H.-B. Schüttler and A. J. Fedro, Phys. Rev. B **38**, 9063 (1988).
[19] K. G. Wilson, Rev. Mod. Phys. **47**, 773 (1975).
[20] H. R. Krishna-murthy, J. W. Wilkins, and K. G. Wilson, Phys. Rev. B **21**, 1003 (1980); **21**, 1044 (1980).
[21] R. Bulla, T. A. Costi, and T. Pruschke, Rev. Mod. Phys. **80**, 395 (2008).
[22] A. J. Leggett, S. Chakravarty, A. T. Dorsey, M. P. A. Fisher, A. Garg, and W. Zwerger, Rev. Mod. Phys. **59**, 1 (1987); U. Weiss, *Quantum Dissipative Systems* (World Scientific, Singapore, 1999).
[23] A. Garg, J. N. Onuchic, and V. Ambegaokar, J. Chem. Phys. **83**, 4491 (1985); J. N. Onuchic, *ibid.* **86**, 3925 (1987); D. G. Evans, R. D. Coalson, H. J. Kim, and Yu. Dakhnovskii, Phys. Rev. Lett. **75**, 3649 (1995).
[24] A. Recati, P. O. Fedichev, W. Zwerger, J. von Delft, and P. Zoller, Phys. Rev. Lett. **94**, 040404 (2005).
[25] K. Le Hur and M.-R. Li, Phys. Rev. B **72**, 073305 (2005).
[26] T. A. Costi and R. H. McKenzie, Phys. Rev. A **68**, 034301 (2003); A. N. Jordan and M. Büttiker, Phys. Rev. Lett. **92**, 247901 (2004); T. Stauber and F. Guinea, Phys. Rev. A **73**, 042110 (2006); A. Kopp, X. Jia, and S. Chakravarty, Ann. Phys. (N.Y.) **322**, 1466 (2007); A. Kopp and K. Le Hur, Phys. Rev. Lett. **98**, 220401 (2007); K. Le Hur, Ann. Phys. (N.Y.) **323**, 2208 (2008).
[27] K. Le Hur, P. Doucet-Beaupré, and W. Hofstetter, Phys. Rev. Lett. **99**, 126801 (2007).
[28] H. Spohn and R. Dümcke, J. Stat. Phys. **41**, 389 (1985); S. K. Kehrein and A. Mielke, Phys. Lett. A **219**, 313 (1996).
[29] R. Bulla, N.-H. Tong, and M. Vojta, Phys. Rev. Lett. **91**, 170601 (2003); R. Bulla, H.-J. Lee, N.-H. Tong, and M. Vojta, Phys. Rev. B **71**, 045122 (2005).
[30] F. B. Anders, R. Bulla, and M. Vojta, Phys. Rev. Lett. **98**, 210402 (2007).
[31] M. Vojta, N.-H. Tong, and R. Bulla, Phys. Rev. Lett. **94**, 070604 (2005).
[32] A. Alvermann and H. Fehske, Phys. Rev. Lett. **102**, 150601 (2009).
[33] A. M. Sengupta, Phys. Rev. B **61**, 4041 (2000).

[34] Q. Si, S. Rabello, K. Ingersent, and J. L. Smith, Nature (London) **413**, 804 (2001); Phys. Rev. B **68**, 115103 (2003); M. T. Glossop and K. Ingersent, Phys. Rev. Lett. **99**, 227203 (2007); J.-X. Zhu, S. Kirchner, R. Bulla, and Q. Si, *ibid.* **99**, 227204 (2007).

[35] K. Le Hur, Phys. Rev. Lett. **92**, 196804 (2004); M.-R. Li and K. Le Hur, *ibid.* **93**, 176802 (2004); M.-R. Li, K. Le Hur, and W. Hofstetter, *ibid.* **95**, 086406 (2005); L. Borda, G. Zaránd, and P. Simon, Phys. Rev. B **72**, 155311 (2005).

[36] S. Kirchner, L. Zhu, Q. Si, and D. Natelson, Proc. Natl. Acad. Sci. U.S.A. **102**, 18824 (2005); S. Kirchner and Q. Si, arXiv:0805.3717 (unpublished).

[37] L. Zhu and Q. Si, Phys. Rev. B **66**, 024426 (2002); G. Zaránd and E. Demler, *ibid.* **66**, 024427 (2002).

[38] M. T. Glossop and K. Ingersent, Phys. Rev. Lett. **95**, 067202 (2005).

[39] M. T. Glossop and K. Ingersent, Phys. Rev. B **75**, 104410 (2007).

[40] C.-H. Chung, M. T. Glossop, L. Fritz, M. Kirćan, K. Ingersent, and M. Vojta, Phys. Rev. B **76**, 235103 (2007); M. T. Glossop, N. Khoshkhou, and K. Ingersent, Physica B **403**, 1303 (2008).

[41] P. M. Riseborough, in *Proceedings of the International Conference on Valence Instabilities and Related Narrow-Band Phenomena, Rochester, NY, 1976*, edited by R. D. Parks (Plenum, New York, 1977), p. 405.

[42] F. D. M. Haldane, Phys. Rev. B **15**, 281 (1977).

[43] F. D. M. Haldane, Phys. Rev. B **15**, 2477 (1977).

[44] A. C. Hewson and D. M. Newns, J. Phys. C **13**, 4477 (1980).

[45] J. L. Smith and Q. Si, Europhys. Lett. **45**, 228 (1999).

[46] J. L. Smith and Q. Si, Phys. Rev. B **61**, 5184 (2000).

[47] H. Kajueter, Ph.D. thesis, Rutgers University, 1996; Q. Si and J. L. Smith, Phys. Rev. Lett. **77**, 3391 (1996); R. Chitra and G. Kotliar, *ibid.* **84**, 3678 (2000).

[48] A. Georges, G. Kotliar, W. Krauth, and M. J. Rozenberg, Rev. Mod. Phys. **68**, 13 (1996).

[49] M. E. Fisher, S.-K. Ma, and B. G. Nickel, Phys. Rev. Lett. **29**, 917 (1972); E. Luijten and H. W. J. Blöte, *ibid.* **76**, 1557 (1996); Phys. Rev. B **56**, 8945 (1997).

[50] A. Winter, H. Rieger, M. Vojta, and R. Bulla, Phys. Rev. Lett. **102**, 030601 (2009).

[51] S. Kirchner, Q. Si, and K. Ingersent, Phys. Rev. Lett. **102**, 166405 (2009); M. Vojta, N.-H. Tong, and R. Bulla, *ibid.* **102**, 249904(E) (2009).

[52] K. Ingersent and Q. Si, Phys. Rev. Lett. **89**, 076403 (2002).

[53] B. A. Jones, C. M. Varma, and J. W. Wilkins, Phys. Rev. Lett. **61**, 125 (1988).

[54] J. R. Schrieffer and P. A. Wolff, Phys. Rev. **149**, 491 (1966).

[55] I. G. Lang and Yu. A. Firsov, Zh. Eksp. Teor. Fiz. **43**, 1843 (1962) [Sov. Phys. JETP **16**, 1301 (1963)].

[56] A number of the results presented in Sec. IV were obtained using unphysically large values of the hybridization width Γ. These values were employed to accelerate the convergence of the NRG levels to the critical spectrum, and thereby to minimize computational rounding errors.

[57] This decomposition of the BFK critical spectrum was not explicitly noted in Refs. 38 and 39. However, it can be understood (following arguments analogous to those presented here for the charge-coupled BFA model) under the assumption that, near the phase boundary, the longitudinal exchange coupling renormalizes rapidly to $J_z=\infty$.

[58] S. Sachdev, Z. Phys. B: Condens. Matter **94**, 469 (1994).

[59] O. Sakai, Y. Shimizu, and T. Kasuya, J. Phys. Soc. Jpn. **58**, 3666 (1989); R. Bulla, T. A. Costi, and D. Vollhardt, Phys. Rev. B **64**, 045103 (2001).

[60] T. A. Costi, A. C. Hewson, and V. Zlatić, J. Phys.: Condens. Matter **6**, 2519 (1994).

[61] From Eqs. (58) and (76), and Tables II and III, one expects the vanishing of $\Gamma_K \propto T_*$ and of $4/\chi_{c,\mathrm{loc}}(0,0)$ on approach to the critical point to be governed by different powers of $\lambda_c - \lambda$.